Eur. Phys. J. C 49, 523–544 (2007)
DOI 10.1140/epjc/s10052-006-0164-8

THE EUROPEAN
PHYSICAL JOURNAL C

Regular Article – Experimental Physics

Measurement of neutral current cross sections at high Bjorken-x with the ZEUS detector at HERA

The ZEUS Collaboration

S. Chekanov[1], M. Derrick[1], S. Magill[1], S. Miglioranzi[1,53], B. Musgrave[1], D. Nicholass[1,53], J. Repond[1], R. Yoshida[1], M.C.K. Mattingly[2], N. Pavel[3,a], A.G.Y. Molina[3], S. Antonelli[4], P. Antonioli[4], G. Bari[4], M. Basile[4], L. Bellagamba[4], M. Bindi[4], D. Boscherini[4], A. Bruni[4], G. Bruni[4], L. Cifarelli[4], F. Cindolo[4], A. Contin[4], M. Corradi[4,54,b], S. De Pasquale[4], G. Iacobucci[4], A. Margotti[4], R. Nania[4], A. Polini[4], L. Rinaldi[4], G. Sartorelli[4], A. Zichichi[4], G. Aghuzumtsyan[5], D. Bartsch[5], I. Brock[5], S. Goers[5], H. Hartmann[5], E. Hilger[5], H.-P. Jakob[5], M. Jüngst[5], O.M. Kind[5], E. Paul[5,c], J. Rautenberg[5,55], R. Renner[5], U. Samson[5,d], V. Schönberg[5], M. Wang[5], M. Wlasenko[5], N.H. Brook[6], G.P. Heath[6], J.D. Morris[6], T. Namsoo[6], M. Capua[7], S. Fazio[7], A. Mastroberardino[7], M. Schioppa[7], G. Susinno[7], E. Tassi[7], J.Y. Kim[8,e], K.J. Ma[8,f], Z.A. Ibrahim[9], B. Kamaluddin[9], W.A.T. Wan Abdullah[9], Y. Ning[10], Z. Ren[10], F. Sciulli[10], J. Chwastowski[11], A. Eskreys[11], J. Figiel[11], A. Galas[11], M. Gil[11], K. Olkiewicz[11], P. Stopa[11], L. Zawiejski[11], L. Adamczyk[12], T. Bołd[12], I. Grabowska-Bołd[12], D. Kisielewska[12], J. Łukasik[12], M. Przybycień[12], L. Suszycki[12], A. Kotański[13,g], W. Słomiński[13], V. Adler[14], U. Behrens[14], I. Bloch[14], A. Bonato[14], K. Borras[14], N. Coppola[14], J. Fourletova[14], A. Geiser[14], D. Gladkov[14], P. Göttlicher[14,56], I. Gregor[14], O. Gutsche[14], T. Haas[14], W. Hain[14], C. Horn[14], B. Kahle[14], U. Kötz[14], H. Kowalski[14], H. Lim[14,57], E. Lobodzinska[14], B. Löhr[14], R. Mankel[14], I.-A. Melzer-Pellmann[14], A. Montanari[14], C.N. Nguyen[14], D. Notz[14], A.E. Nuncio-Quiroz[14], R. Santamarta[14], U. Schneekloth[14], A. Spiridonov[14,58], H. Stadie[14], U. Stösslein[14], D. Szuba[14,59], J. Szuba[14,60], T. Theedt[14], G. Watt[14], G. Wolf[14], K. Wrona[14], C. Youngman[14], W. Zeuner[14], S. Schlenstedt[15], G. Barbagli[16], E. Gallo[16], P.G. Pelfer[16], A. Bamberger[17], D. Dobur[17], F. Karstens[17], N.N. Vlasov[17,h], P.J. Bussey[18], A.T. Doyle[18], W. Dunne[18], J. Ferrando[18], D.H. Saxon[18], I.O. Skillicorn[18], I. Gialas[19,61], T. Gosau[20], U. Holm[20], R. Klanner[20], E. Lohrmann[20], H. Salehi[20], P. Schleper[20], T. Schörner-Sadenius[20], J. Sztuk[20], K. Wichmann[20], K. Wick[20], M. Kataoka[22,62], T. Matsumoto[22], K. Nagano[22], K. Tokushuku[22,63], S. Yamada[22], Y. Yamazaki[22], C. Foudas[21], C. Fry[21], K.R. Long[21], A.D. Tapper[21], A.N. Barakbaev[23], E.G. Boos[23], A. Dossanov[23], N.S. Pokrovskiy[23], B.O. Zhautykov[23], D. Son[24], J. de Favereau[25], K. Piotrzkowski[25], F. Barreiro[26], C. Glasman[26,i], M. Jimenez[26], L. Labarga[26], J. del Peso[26], E. Ron[26], J. Terrón[26], M. Zambrana[26], F. Corriveau[27], C. Liu[27], R. Walsh[27], C. Zhou[27], T. Tsurugai[28], A. Antonov[29], B.A. Dolgoshein[29], I. Rubinsky[29], V. Sosnovtsev[29], A. Stifutkin[29], S. Suchkov[29], R.K. Dementiev[30], P.F. Ermolov[30], L.K. Gladilin[30], I.I. Katkov[30], L.A. Khein[30], I.A. Korzhavina[30], V.A. Kuzmin[30], B.B. Levchenko[30,j], O.Y. Lukina[30], A.S. Proskuryakov[30], L.M. Shcheglova[30], D.S. Zotkin[30], S.A. Zotkin[30], I. Abt[31], C. Büttner[31], A. Caldwell[31], D. Kollar[31], W.B. Schmidke[31], J. Sutiak[31], G. Grigorescu[32], A. Keramidas[32], E. Koffeman[32], P. Kooijman[32], A. Pellegrino[32], H. Tiecke[32], M. Vázquez[32,64], L. Wiggers[32], N. Brümmer[33], B. Bylsma[33], L.S. Durkin[33], A. Lee[33], T.Y. Ling[33], P.D. Allfrey[34], M.A. Bell[34], A.M. Cooper-Sarkar[34], A. Cottrell[34], R.C.E. Devenish[34], B. Foster[34], C. Gwenlan[34,k], K. Korcsak-Gorzo[34], S. Patel[34], V. Roberfroid[34,l], A. Robertson[34], P.B. Straub[34], C. Uribe-Estrada[34], R. Walczak[34], P. Bellan[35], A. Bertolin[35], R. Brugnera[35], R. Carlin[35], R. Ciesielski[35], F. Dal Corso[35], S. Dusini[35], A. Garfagnini[35], S. Limentani[35], A. Longhin[35], L. Stanco[35], M. Turcato[35], B.Y. Oh[36], A. Raval[36], J.J. Whitmore[36], Y. Iga[37], G. D'Agostini[38], G. Marini[38], A. Nigro[38], J.E. Cole[39], J.C. Hart[39], H. Abramowicz[39,65], A. Gabareen[39], R. Ingbir[39], S. Kananov[39], A. Levy[39], M. Kuze[41], R. Hori[42], S. Kagawa[42,66], S. Shimizu[42], T. Tawara[42], R. Hamatsu[43], H. Kaji[43], S. Kitamura[43,67], O. Ota[43], Y.D. Ri[43], M.I. Ferrero[44], V. Monaco[44], R. Sacchi[44], A. Solano[44], M. Arneodo[45], M. Ruspa[45], S. Fourletov[46], J.F. Martin[46], S.K. Boutle[47,61], J.M. Butterworth[47], R. Hall-Wilton[47,64], T.W. Jones[47], J.H. Loizides[47], M.R. Sutton[47,m], C. Targett-Adams[47], M. Wing[47], B. Brzozowska[48], J. Ciborowski[48,68], G. Grzelak[48], P. Kulinski[48], P. Łużniak[48,69], J. Malka[48,69], R.J. Nowak[48], J.M. Pawlak[48], T. Tymieniecka[48], A. Ukleja[48,n], J. Ukleja[48,o], A.F. Żarnecki[48], M. Adamus[49], P. Plucinski[49,p], Y. Eisenberg[50], I. Giller[50], D. Hochman[50], U. Karshon[50], M. Rosin[50], E. Brownson[51], T. Danielson[51], A. Everett[51], D. Kçira[51], D.D. Reeder[51], P. Ryan[51], A.A. Savin[51], W.H. Smith[51], H. Wolfe[51], S. Bhadra[52], C.D. Catterall[52], Y. Cui[52], G. Hartner[52], S. Menary[52], U. Noor[52], M. Soares[52], J. Standage[52], J. Whyte[52]

[1] Argonne National Laboratory, Argonne, Illinois 60439-4815, USA[q]
[2] Andrews University, Berrien Springs, Michigan 49104-0380, USA
[3] Institut für Physik der Humboldt-Universität zu Berlin, Berlin, Germany
[4] University and INFN Bologna, Bologna, Italy[r]
[5] Physikalisches Institut der Universität Bonn, Bonn, Germany[s]

[6] H.H. Wills Physics Laboratory, University of Bristol, Bristol, UK[t]
[7] Calabria University, Physics Department and INFN, Cosenza, Italy[q]
[8] Chonnam National University, Kwangju, South Korea[u]
[9] Jabatan Fizik, Universiti Malaya, 50603 Kuala Lumpur, Malaysia[v]
[10] Nevis Laboratories, Columbia University, Irvington on Hudson, New York 10027, USA[w]
[11] The Henryk Niewodniczanski Institute of Nuclear Physics, Polish Academy of Sciences, Cracow, Poland[x]
[12] Faculty of Physics and Applied Computer Science, AGH-University of Science and Technology, Cracow, Poland[y]
[13] Department of Physics, Jagellonian University, Cracow, Poland
[14] Deutsches Elektronen-Synchrotron DESY, Hamburg, Germany
[15] Deutsches Elektronen-Synchrotron DESY, Zeuthen, Germany
[16] University and INFN, Florence, Italy[q]
[17] Fakultät für Physik der Universität Freiburg i.Br., Freiburg i.Br., Germany[r]
[18] Department of Physics and Astronomy, University of Glasgow, Glasgow, UK[s]
[19] Department of Engineering in Management and Finance, Univ. of Aegean, Greece
[20] Hamburg University, Institute of Exp. Physics, Hamburg, Germany[r]
[21] Imperial College London, High Energy Nuclear Physics Group, London, UK[s]
[22] Institute of Particle and Nuclear Studies, KEK, Tsukuba, Japan[z]
[23] Institute of Physics and Technology of Ministry of Education and Science of Kazakhstan, Almaty Kazakhstan
[24] Kyungpook National University, Center for High Energy Physics, Daegu, South Korea[t]
[25] Institut de Physique Nucléaire, Université Catholique de Louvain, Louvain-la-Neuve, Belgium[aa]
[26] Departamento de Física Teórica, Universidad Autónoma de Madrid, Madrid, Spain[ab]
[27] Department of Physics, McGill University, Montréal, Québec, Canada H3A 2T8[ag]
[28] Meiji Gakuin University, Faculty of General Education, Yokohama, Japan[y]
[29] Moscow Engineering Physics Institute, Moscow, Russia[ac]
[30] Moscow State University, Institute of Nuclear Physics, Moscow, Russia[ad]
[31] Max-Planck-Institut für Physik, München, Germany
[32] NIKHEF and University of Amsterdam, Amsterdam, Netherlands[ae]
[33] Physics Department, Ohio State University, Columbus, Ohio 43210, USA[p]
[34] Department of Physics, University of Oxford, Oxford, UK[s]
[35] Dipartimento di Fisica dell' Università and INFN, Padova, Italy[q]
[36] Department of Physics, Pennsylvania State University, University Park, Pennsylvania 16802, USA[v]
[37] Polytechnic University, Sagamihara, Japan[y]
[38] Dipartimento di Fisica, Università 'La Sapienza' and INFN, Rome, Italy[q]
[39] Rutherford Appleton Laboratory, Chilton, Didcot, Oxon, UK[s]
[40] Raymond and Beverly Sackler Faculty of Exact Sciences, School of Physics, Tel-Aviv University, Tel-Aviv, Israel[af]
[41] Department of Physics, Tokyo Institute of Technology, Tokyo, Japan[y]
[42] Department of Physics, University of Tokyo, Tokyo, Japan[y]
[43] Tokyo Metropolitan University, Department of Physics, Tokyo, Japan[y]
[44] Università di Torino and INFN, Torino, Italy[q]
[45] Università del Piemonte Orientale, Novara, and INFN, Torino, Italy[q]
[46] Department of Physics, University of Toronto, Toronto, Ontario, Canada M5S 1A7[a]
[47] Physics and Astronomy Department, University College London, London, UK[s]
[48] Warsaw University, Institute of Experimental Physics, Warsaw, Poland
[49] Institute for Nuclear Studies, Warsaw, Poland
[50] Department of Particle Physics, Weizmann Institute, Rehovot, Israel[ag]
[51] Department of Physics, University of Wisconsin, Madison, Wisconsin 53706, USA[p]
[52] Department of Physics, York University, Ontario, Canada M3J 1P3[ah]
[53] also affiliated with University College London, UK
[54] also at University of Hamburg, Germany, Alexander von Humboldt Fellow
[55] now at Univ. of Wuppertal, Germany
[56] now at DESY group FEB, Hamburg, Germany
[57] now at Argonne National Laboratory, Argonne, IL, USA
[58] also at Institut of Theoretical and Experimental Physics, Moscow, Russia
[59] also at INP, Cracow, Poland
[60] on leave of absence from FPACS, AGH-UST, Cracow, Poland
[61] also affiliated with DESY
[62] now at ICEPP, University of Tokyo, Japan
[63] also at University of Tokyo, Japan
[64] now at CERN, Geneva, Switzerland
[65] also at Max Planck Institute, Munich, Germany, Alexander von Humboldt Research Award
[66] now at KEK, Tsukuba, Japan
[67] Tokyo Metropolitan University, Department of Radiological Science, Tokyo, Japan

[68] also at Łódź University, Poland
[69] Łódź University, Poland

Received: 2 August 2006 / Revised version: 21 October 2006 /

Abstract. A new method is employed to measure the neutral current cross section up to Bjorken-x values of one with the ZEUS detector at HERA using an integrated luminosity of 65.1 pb^{-1} for e^+p collisions and 16.7 pb^{-1} for e^-p collisions at $\sqrt{s} = 318$ GeV and 38.6 pb^{-1} for e^+p collisions at $\sqrt{s} = 300$ GeV. Cross sections have been extracted for $Q^2 \geq 648\ \text{GeV}^2$ and are compared to predictions using different parton density functions. For the highest x bins, the data have a tendency to lie above the expectations using recent parton density function parametrizations.

1 Introduction

Only limited information is available on structure functions at high Bjorken-x in the deep inelastic scattering (DIS) regime. This is largely due to limitations in beam energies, in measurement techniques and the small cross section at high x. In this paper, a new method is described and used to measure the neutral current (NC) cross section in electron–proton scattering up to $x = 1$ with data from the ZEUS detector at HERA.

At HERA, proton beams of 920 GeV (820 GeV prior to 1998), collide with either electron or positron beams of 27.5 GeV. The electron[1] interacts with the proton via the exchange of a gauge boson.

The description of DIS is usually given in terms of three Lorentz-invariant quantities, Q^2, x and y, which are related by $Q^2 = sxy$, where the masses of the electron and proton are neglected, s is the square of the center-of-mass energy, Q^2 is the negative of the square of the transferred four-momentum, x is the Bjorken variable [1] and y is the inelasticity. The NC electron–proton differential scattering cross section is typically written in terms of the proton structure functions as

$$\frac{\mathrm{d}^2\sigma^{\mathrm{SM}}_{\mathrm{Born}}(e^\pm p)}{\mathrm{d}x\,\mathrm{d}Q^2} = \frac{2\pi\alpha^2}{xQ^4}\left[Y_+F_2\left(x,Q^2\right) \mp Y_-xF_3\left(x,Q^2\right) - y^2F_L\left(x,Q^2\right)\right], \qquad (1)$$

---

[a] deceased

[b] e-mail: corradi@mail.desy.de

[c] retired

[d] formerly U. Meyer

[e] supported by Chonnam National University in 2005

[f] supported by a scholarship of the World Laboratory Björn Wiik Research Project

[g] supported by the research grant no. 1 P03B 04529 (2005-2008)

[h] partly supported by Moscow State University, Russia

[i] Ramón y Cajal Fellow

[j] partly supported by Russian Foundation for Basic Research grant no. 05-02-39028-NSFC-a

[k] PPARC Postdoctoral Research Fellow

[l] EU Marie Curie Fellow

[m] PPARC Advanced fellow

[n] supported by the Polish Ministry for Education and Science grant no. 1 P03B 12629

[o] supported by the KBN grant no. 2 P03B 12725

[p] supported by the Polish Ministry for Education and Science grant no. 1 P03B 14129

[q] supported by the US Department of Energy

[r] supported by the Italian National Institute for Nuclear Physics (INFN)

[s] supported by the German Federal Ministry for Education and Research (BMBF), under contract numbers HZ1GUA 2, HZ1GUB 0, HZ1PDA 5, HZ1VFA 5

[t] supported by the Particle Physics and Astronomy Research Council, UK

[u] supported by the Korean Ministry of Education and Korea Science and Engineering Foundation

[v] supported by the Malaysian Ministry of Science, Technology and Innovation/Akademi Sains Malaysia grant SAGA 66-02-03-0048

[w] supported by the US National Science Foundation

[x] supported by the Polish State Committee for Scientific Research, grant no. 620/E-77/SPB/DESY/P-03/DZ 117/2003-2005 and grant no. 1P03B07427/2004-2006

[y] supported by the Polish Ministry of Scientific Research and Information Technology, grant no. 112/E-356/SPUB/DESY/P-03/DZ 116/2003-2005 and 1 P03B 065 27

[z] supported by the Japanese Ministry of Education, Culture, Sports, Science and Technology (MEXT) and its grants for Scientific Research

[aa] supported by FNRS and its associated funds (IISN and FRIA) and by an Inter-University Attraction Poles Programme subsidised by the Belgian Federal Science Policy Office

[ab] supported by the Spanish Ministry of Education and Science through funds provided by CICYT

[ac] partially supported by the German Federal Ministry for Education and Research (BMBF)

[ad] supported by RF Presidential grant N 1685.2003.2 for the leading scientific schools and by the Russian Ministry of Education and Science through its grant for Scientific Research on High Energy Physics

[ae] supported by the Netherlands Foundation for Research on Matter (FOM)

[af] supported by the German-Israeli Foundation and the Israel Science Foundation

[ag] supported in part by the MINERVA Gesellschaft für Forschung GmbH, the Israel Science Foundation (grant no. 293/02-11.2) and the U.S.-Israel Binational Science Foundation

[ah] supported by the Natural Sciences and Engineering Research Council of Canada (NSERC)

[1] In the following, we use the term electron to represent both electrons and positrons unless specifically noted otherwise.

where $Y_\pm \equiv 1 \pm (1-y)^2$ and α denotes the fine-structure constant. At leading order (LO) in QCD, the longitudinal structure function, F_L, is zero and the structure functions F_2 and xF_3 can be expressed as products of electroweak couplings and parton density functions (PDFs).

The form of the PDFs is typically parametrized as $q(x) = Ax^{-\lambda} f(x)(1-x)^\eta$, where $f(x)$ interpolates between the low-x and high-x domains. Such a form allows for an accurate description of the data at low x [2–6]. For $x \geq 0.3$, the PDFs are found to decrease very quickly. However, a direct confrontation with data has not been possible to date for $x \to 1$. The highest measured points in the DIS regime are for $x = 0.75$ [7]. Data at higher x exist [8, 9] but these are in the resonance production region and cannot be easily interpreted in terms of parton distributions. The highest x value for HERA structure function data reported to date is $x = 0.65$ [4, 5]. The differences between different PDF sets increase rapidly as x increases, even though they use similar data and have common parametrization for $x \to 1$. The uncertainties for $x > 0.75$ are large and hard to quantify.

This paper presents a reanalysis of previously published ZEUS data [4, 10, 11] with a new reconstruction technique designed to extract cross sections extending up to $x = 1$ at high Q^2. The data correspond to an integrated luminosity of 38.6 pb^{-1} for e^+p collisions at $\sqrt{s} = 300$ GeV recorded in 96–97, 16.7 pb^{-1} for e^-p collisions at $\sqrt{s} = 318$ GeV recorded in 98–99 and 65.1 pb^{-1} for e^+p collisions at $\sqrt{s} = 318$ GeV recorded in 99–00.

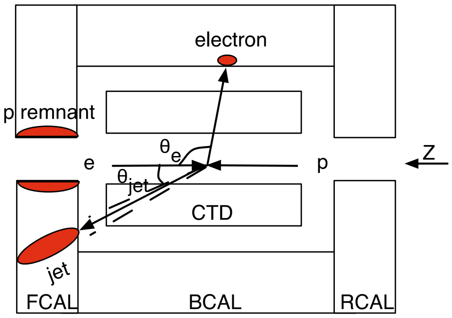

Fig. 1. A schematic depiction of the ZEUS detector with the main components used in this analysis labeled. Also shown is a typical topology for events studied in this analysis. The electron is scattered at a large angle and is reconstructed using the central tracking detector (CTD) and the barrel calorimeter (BCAL), while the scattered jet is typically reconstructed in the forward calorimeter (FCAL). The jet of particles from the proton remnant mostly disappears down the beam pipe

2 The ZEUS experiment at HERA

ZEUS is a multipurpose detector described elsewhere [12]. A schematic depiction of the ZEUS detector is given in Fig. 1. A brief outline of the components that are most relevant for this analysis is given below.

The high-resolution uranium–scintillator calorimeter (CAL) [13–16] consists of three parts: the forward (FCAL), the barrel (BCAL) and the rear (RCAL) calorimeters. Each part is divided into modules and further subdivided into towers; each tower is longitudinally segmented into one electromagnetic section (EMC) and either one (in RCAL) or two (in BCAL and FCAL) hadronic sections (HAC). The smallest subdivision of the calorimeter is called a cell. The CAL energy resolutions, measured under test-beam conditions, are $\sigma(E)/E = 0.18/\sqrt{E}$ for electrons and $\sigma(E)/E = 0.35/\sqrt{E}$ for hadrons, with E in GeV. The timing resolution of the CAL is ~ 1 ns for energy deposits larger than 4.5 GeV.

Charged particles are tracked in the central tracking detector (CTD) [17–19], which operates in a magnetic field of 1.43 T provided by a thin superconducting solenoid. The CTD consists of 72 cylindrical drift-chamber layers, organized in nine superlayers covering the polar-angle[2] region $15° < \theta < 164°$. The transverse-momentum resolution for full-length tracks is $\sigma(p_\text{T})/p_\text{T} = 0.0058\, p_\text{T} \oplus 0.0065 \oplus 0.0014/p_\text{T}$, with p_T in GeV.

The luminosity is measured using the Bethe–Heitler reaction $ep \to e\gamma p$ [20–22]. The resulting small-angle photons were measured by the luminosity monitor, a lead-scintillator calorimeter placed in the HERA tunnel 107 m from the interaction point in the electron beam direction.

3 New reconstruction method

Figure 1 also shows a schematic depiction of a high-Q^2 NC event in the ZEUS detector: a scattered electron and a jet are outlined in the CAL, while the proton remnant largely disappears down the forward beam pipe. The electron is typically scattered at a large angle and is easily recognized in the detector.

Such events have been analyzed by a variety of techniques in the past, such as the double-angle method, all of which limited the maximum value of x which could be measured. In the new techniques presented here, the hadronic system can be used to measure x by reconstructing the energy and angle of the jet produced by the scattered quark. Above some x value that depends on Q^2, the jet is at a small angle and not well reconstructed. An integrated cross section above an x cut value is then measured.

The scattered electron was identified and reconstructed by combining calorimeter and CTD information [23]. The algorithm starts by identifying CAL clusters topologically consistent with an electromagnetic shower. If the electron candidate was in the range $23° < \theta_\text{e} < 156°$, a well reconstructed matched track was required. The scattered-electron energy, E'_e, was determined from the calorime-

---

[2] The ZEUS coordinate system is a right-handed Cartesian system, with the Z axis pointing in the proton beam direction, referred to as the “forward direction”, and the X axis pointing left towards the center of HERA. The coordinate origin is at the nominal interaction point.

ter energy deposit and was corrected for the energy lost in inactive material in front of the CAL. The electron energy resolution was 5% for $E'_\mathrm{e} > 20\,\mathrm{GeV}$. The electron angle θ_e was determined using the matched track, when available, and the position of the calorimeter cluster and the event vertex if the electron was outside the CTD acceptance. The electron angular resolution was 2 mrad for $\theta_\mathrm{e} < 23°$, 3 mrad for $23° < \theta_\mathrm{e} < 156°$ and 5 mrad for $\theta_\mathrm{e} > 156°$ [4].

Jets were reconstructed from the remaining clusters with the longitudinally invariant k_T cluster algorithm [24] in the inclusive mode [25]. Each cluster energy was corrected for energy loss in dead material, and clusters identified as backsplash [23] from the FCAL into the BCAL or RCAL were rejected. The jet variables were defined according to the Snowmass convention [26]:

$$E_{\mathrm{T,jet}} = \sum_i E_{\mathrm{T},i}\,, \quad \eta_{\mathrm{jet}} = \frac{\sum_i E_{\mathrm{T},i}\eta_i}{E_{\mathrm{T,jet}}}\,,$$

$$\theta_{\mathrm{jet}} = 2\tan^{-1}(e^{-\eta_{\mathrm{jet}}})\,, \quad E_{\mathrm{jet}} = \sum_i E_i,$$

where E_i, $E_{\mathrm{T},i}$ and η_i are the energy, transverse energy and pseudorapidity of the CAL clusters. The jet energy and angular resolutions were $\sigma_{E_\mathrm{jet}}/E_\mathrm{jet} = 55\%/\sqrt{E_\mathrm{jet}} \oplus 2\%$ and $\sigma_{\theta_\mathrm{jet}}/\theta_\mathrm{jet} = 1.6\% \oplus 1.9\%/\sqrt{\theta_\mathrm{jet}}$ [27].

Events were first sorted into Q^2 bins using information from the electron only:

$$Q^2 = 2E_\mathrm{e}E'_\mathrm{e}(1+\cos\theta_\mathrm{e})\,,$$

where E_e is the electron beam energy. The electron was well reconstructed in the whole kinematic region, yielding a relative resolution in Q^2 for all x of about 5%. The jet information was then used to calculate x for events with a well reconstructed jet:

$$x = \frac{E_\mathrm{jet}(1+\cos\theta_\mathrm{jet})}{2E_p\left(1-\frac{E_\mathrm{jet}(1-\cos\theta_\mathrm{jet})}{2E_e}\right)}\,,$$

where E_p is the proton beam energy. The relative resolution in x varied from 15% to 4% as x increased from 0.06 to 0.7 in events where a jet could be reconstructed. At high x, θ_jet is small and $x \approx E_\mathrm{jet}/E_\mathrm{p}$, where E_jet has good resolution. The events with a reconstructed jet were sorted into x bins to allow a measurement of the double differential cross-section $\mathrm{d}^2\sigma_\mathrm{Born}/\mathrm{d}x\mathrm{d}Q^2$. Events with no jet reconstructed within the fiducial volume were assumed to come from high x and were collected in a bin with $x_\mathrm{edge} < x < 1$. An integrated cross section was calculated from $\int_{x_\mathrm{edge}}^1(\mathrm{d}^2\sigma_\mathrm{Born}/\mathrm{d}x\mathrm{d}Q^2)\mathrm{d}x$. Due to their poorer x resolution, events with more than one jet were discarded. The correction to the cross section for multi-jet events was taken from the Monte Carlo simulation described below, and ranged from 9% at $x = 0.1$ to 1% at $x = 0.6$. The systematic uncertainty associated with this cut is discussed in Sect. 6.2.2. More details of this reconstruction technique are given elsewhere [28].

4 Monte Carlo simulations

Monte Carlo (MC) simulations were used to evaluate the efficiency for selecting events, for determining the accuracy of the kinematic reconstruction, and for estimating the background rate. The statistical uncertainties from the MC samples were negligible in comparison to those of the data.

Standard model (SM) NC DIS events were simulated with DJANGOH version 1.1 [29, 30] which includes an interface to the HERACLES 4.6.1 [31] program. HERACLES includes the corrections for the initial- and final-state electroweak radiation, vertex and propagator corrections, and two-boson exchange. Photon radiation from quarks was included in the simulation. The hadronic final state was simulated using the MEPS model of LEPTO 6.5 [32], which includes order-α_S matrix elements (ME) with a lower and upper cutoff on the soft and collinear divergences. Both the ME cut-offs and the parton evolutions are treated by parton showers based on the DGLAP evolution equations. The fragmentation of the scattered partons into observable hadrons is performed with the Lund string hadronization model by JETSET [33]. The CTEQ6D PDF set [3] was used.

The ZEUS detector response was simulated using a program based on GEANT 3.13 [34]. The generated events were passed through the detector simulation, subjected to the same trigger requirements as the data and processed by the same reconstruction programs.

The vertex distribution in data is a crucial input to the MC simulation for the correct evaluation of the event-selection efficiency. Therefore, the Z-vertex distribution used in the MC simulation was determined from a sample of NC DIS events in which the event-selection efficiency was independent of the Z position of the event vertex [4].

5 Event selection

5.1 Trigger

ZEUS operates a three-level trigger system [4, 35]. At the first-level, only coarse calorimeter and tracking information are available. Events were selected using criteria based on energy deposits in the CAL consistent with an isolated electron. In addition, events with high E_T in coincidence with a CTD track were accepted. At the second level, a cut on $\delta > 29$ GeV was imposed to select NC events, with δ defined as:

$$\delta \equiv \sum_i (E-p_Z)_i = \sum_i (E_i - E_i\cos\theta_i)\,,$$

where the sum runs over all calorimeter energy deposits E_i with polar angles θ_i. Timing information from the calorimeter was used to reject events inconsistent with the bunch-crossing time. At the third level, events were fully reconstructed and selected according to requirements similar to, but looser than, the offline cuts described below.

The main uncertainty in the trigger efficiency comes from the first level. The efficiency in data and MC simulation agreed to within $\sim 0.5\%$ and the overall efficiency was above 95%.

5.2 Offline selection

The following criteria were imposed to select NC DIS events offline:

- an electron with $E'_{\mathrm{e}} > 25\,\mathrm{GeV}$ was required. An isolation cut was imposed by requiring that less than 4 GeV be deposited in calorimeter cells not associated with the scattered electron in an η–ϕ cone of radius $R_{\mathrm{cone}} = 0.8$ centered on the candidate cluster. For those electrons in the CTD acceptance, a matched track was required which passed within 10 cm of the cluster center. The matched track was required to traverse at least four of the nine superlayers of the CTD. The momentum of the track, p_{trk}, had to be at least 10 GeV. For electrons outside the forward tracking acceptance of the CTD, the tracking requirement in the electron selection was replaced by a cut on the transverse momentum of the electron, $p_{\mathrm{T,e}} > 30\,\mathrm{GeV}$;
- a fiducial-volume cut was applied to the electron to guarantee that the experimental acceptance was well understood. It excluded the transition regions between the FCAL and the BCAL [36]. It also excluded the regions within 1.5 cm of the module gaps in the BCAL. As the kinematic region considered in this analysis is at high Q^2, events with electrons in the RCAL were discarded.

The following cuts were used to select an essentially background free and well reconstructed event sample:

- either 0 or 1 valid jets. Valid jets were required to have $E_{\mathrm{T,jet}} > 10\,\mathrm{GeV}$ and $\theta_{\mathrm{jet}} > 0.12\,\mathrm{rad}$;
- a reconstructed vertex with $-50 < Z_{\mathrm{vtx}} < 50\,\mathrm{cm}$, a range consistent with ep interactions;
- $\delta > 40\,\mathrm{GeV}$ to suppress photoproduction events, in which the scattered electron escaped through the beam hole in the RCAL. This cut value was $\delta > 47\,\mathrm{GeV}$ for events in the highest x bins. This cut also rejected events with large initial-state QED radiation. In addition, $\delta < 65\,\mathrm{GeV}$ was required to remove "overlay" events in which a normal DIS event coincided with additional energy deposits in the RCAL from some other reaction. This requirement had a negligible effect on the efficiency for selecting NC DIS events.
- $y_{\mathrm{e}} < 0.95$ to further reduce background from photoproduction events, where y_{e} was defined as

$$y_{\mathrm{e}} = 1 - \frac{E'_{\mathrm{e}}}{2E_{\mathrm{e}}}(1 - \cos\theta_{\mathrm{e}})\,,$$

- $P_{\mathrm{T}}/\sqrt{E_{\mathrm{T}}} < 4\sqrt{\mathrm{GeV}}$ to remove cosmic rays and beam-related backgrounds. The variables P_{T} and E_{T} were defined by:

$$P_{\mathrm{T}}^2 = P_X^2 + P_Y^2 = \left(\sum_i E_i \sin\theta_i \cos\phi_i\right)^2 + \left(\sum_i E_i \sin\theta_i \sin\phi_i\right)^2\,,$$

$$E_{\mathrm{T}} = \sum_i E_i \sin\theta_i\,,$$

  where the sums run over all calorimeter energy deposits, E_i, with polar and azimuthal angles θ_i and ϕ_i with respect to the event vertex, respectively;
- ≥ 5 HAC cells with energy above 110 MeV to remove elastic Compton scattering events ($ep \to e\gamma p$) and further reduce the size of the QED radiative corrections. The contribution from deeply virtual Compton scattering was found to be negligible;
- $y_{\mathrm{JB}} < 1.3 \cdot Q^2_{\mathrm{edge}}/(s \cdot x_{\mathrm{edge}})$ to limit event migration from small x to large x for zero-jet events. The variable y_{JB} was calculated with the Jacquet–Blondel method [37]. The quantities x_{edge} and Q^2_{edge} are the lower x and upper Q^2 edges of the bins defined for the cross-section measurement (see Sect. 6.1).

After these selections, 10298 events remained in the 99–00 e^+p data, 2664 in the 98–99 e^-p data and 5935 in the 96–97 e^+p data in the bins used to extract the cross sections. The numbers of events in the zero-jet bins were 1292, 293 and 493, respectively.

Monte Carlo distributions are compared with those from data in Figs. 2–5 for several variables. The MC distributions are normalized to the measured luminosity. Only the comparison to 99–00 e^+p data is shown; the comparisons of 98–99 e^-p and 96–97 e^+p data with MC distributions show similar features. The first set of plots, Fig. 2, shows general properties for the full sample of events. Good agreement between data and MC simulation is observed,

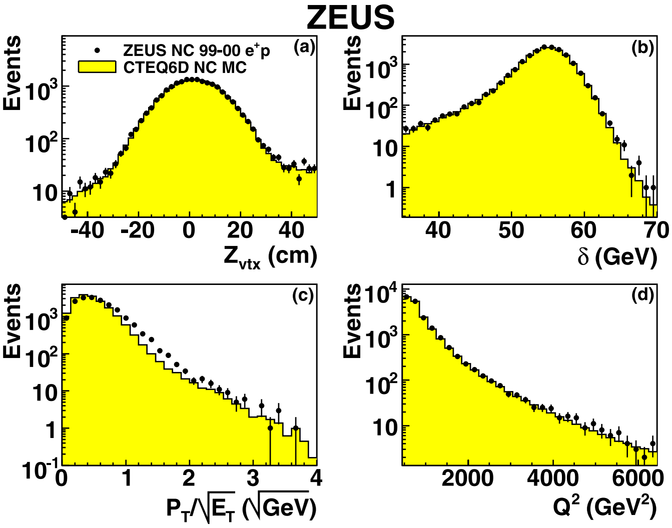

Fig. 2. Comparison of NC MC distributions (*histograms*) with 99–00 e^+p data (*points*) for: **a** the Z coordinate of the event vertex; **b** δ; **c** $P_{\mathrm{T}}/\sqrt{E_{\mathrm{T}}}$ and **d** Q^2. The MC distributions are normalized to the measured luminosity

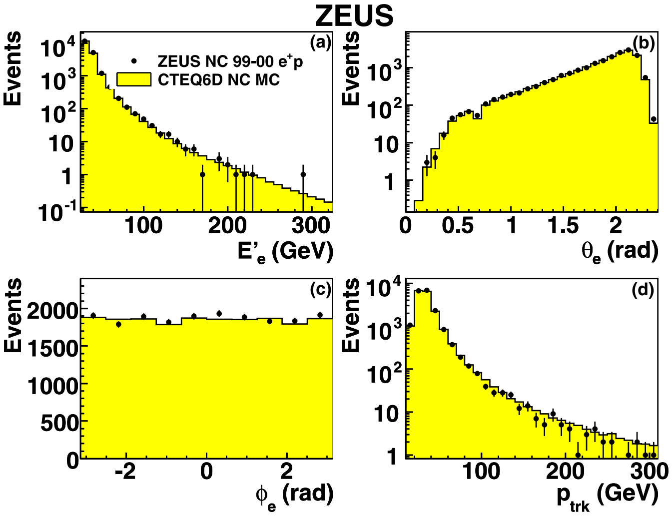

Fig. 3. Comparison of NC MC distributions (*histograms*) with 99–00 e^+p data (*points*) for: **a** E'_{e}; **b** θ_{e}; **c** ϕ_{e} and **d** p_{trk}, the momentum of the track associated with the scattered electron. The MC distributions are normalized to the measured luminosity

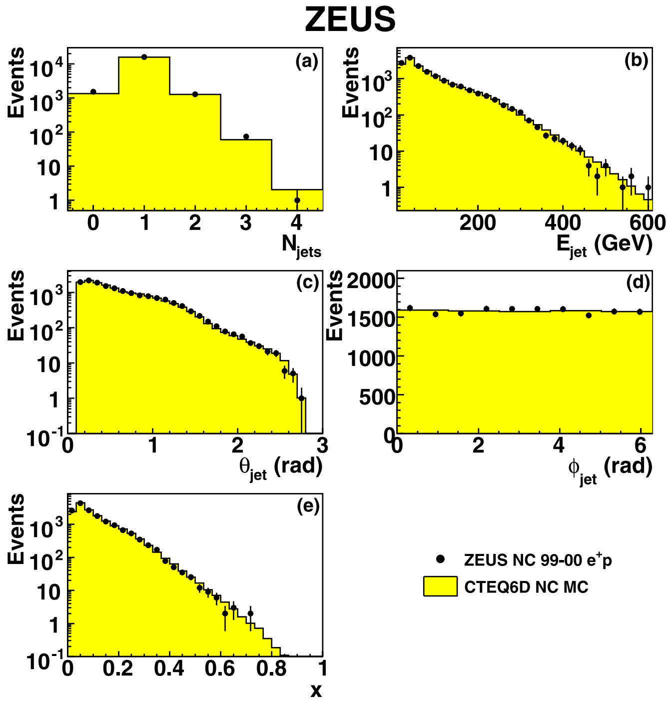

Fig. 4. Comparison of NC MC distributions (*histograms*) with 99–00 e^+p data (*points*) for: **a** the number of reconstructed jets; **b** E_{jet}; **c** θ_{jet}; **d** ϕ_{jet} and **e** x calculated from the jet. The jet distributions are for one jet events. The MC distributions are normalized to the measured luminosity

with no indication of residual backgrounds. The small disagreement observed in Fig. 2c has been verified to have negligible impact on the results presented in this paper. Figure 3 shows distributions related to the scattered electron. Figure 4 presents a series of control plots for jet quantities. The MC reproduces the data distribution for the number of reconstructed jets to high accuracy: the numbers of data events with 0–4 jets were found to be 1292, 15187, 1258, 73 and 2. The Monte Carlo simulation predicted 1163, 15155, 1233, 58 and 1 events. This is important since the MC is used to correct for the inefficiency resulting from the requirement of zero or one jet in the event. The remaining distributions in this figure are for the jet quantities in one jet events. Figure 5 shows distributions for the class of events with zero jets. Overall, 13% more data events for 99–00 e^+p, 2% more data events for 98–99 e^-p and 5% more data events for 96–97 e^+p are observed for zero-jet events than expected in the simulation. An offset in the δ distribution is seen, with the MC distribution slightly lower than the data. This offset can however be explained by shifting the electron energy scale by 1%, which is within its estimated uncertainty.

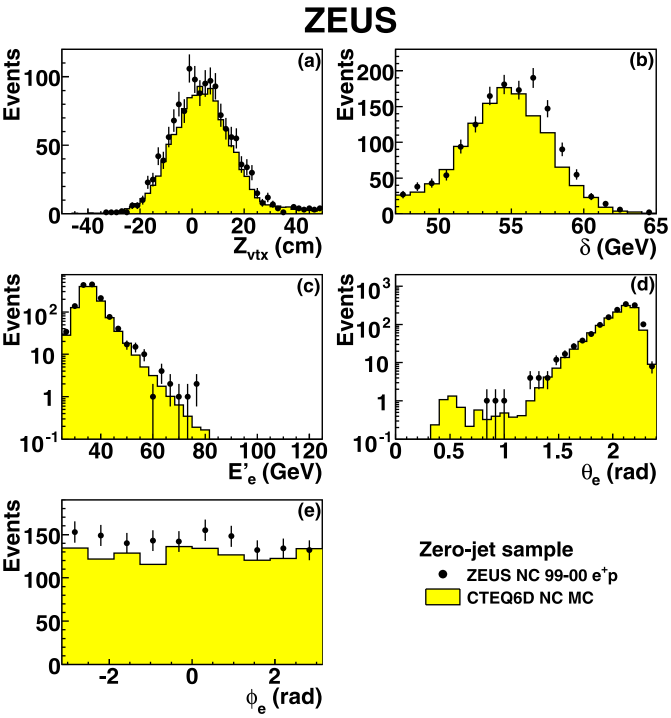

Fig. 5. Comparison of NC MC distributions (*histograms*) with 99–00 e^+p data (*points*) for events with zero jets. The plots show: **a** the Z coordinate of the event vertex; **b** δ; **c** E'_{e}; **d** θ_{e} and **e** ϕ_{e}. The MC distributions are normalized to the measured luminosity

6 Analysis

6.1 Binning, acceptance and cross-section determination

The bins in the (x, Q^2) kinematic space used in this analysis are shown in Fig. 6. The bin widths in Q^2 were chosen to correspond to three times the resolution of the reconstructed Q^2. The minimum value of Q^2 corres-

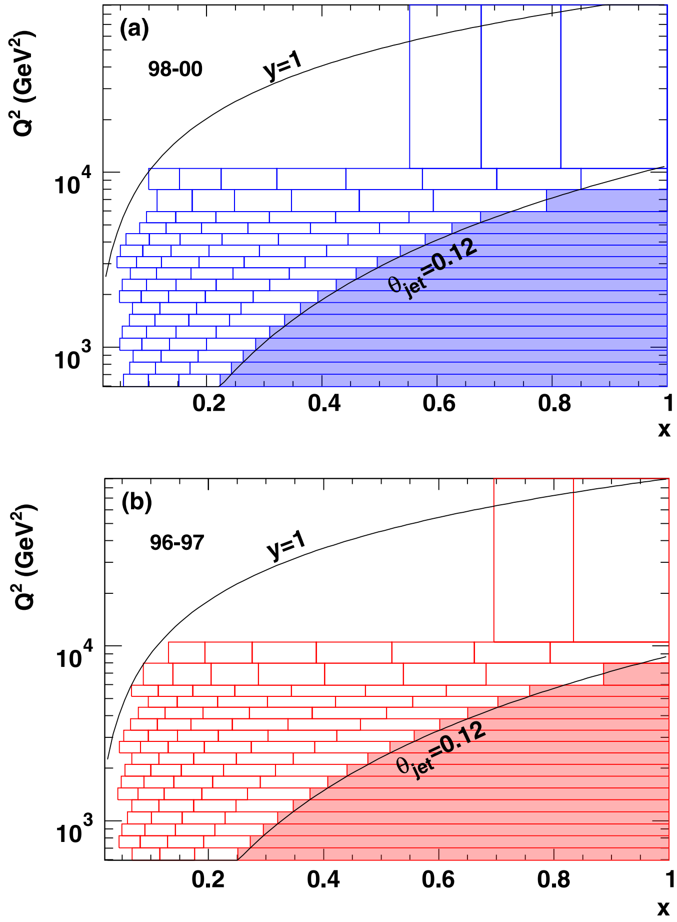

Fig. 6. Definition of the bins as used in this analysis for: **a** 98–00 data with $E_{\mathrm{p}} = 920\,\mathrm{GeV}$ and **b** 96–97 data with $E_{\mathrm{p}} = 820\,\mathrm{GeV}$. The *shaded* bins extending to $x = 1$ are for the zero-jet events. The $y = 1$ *lines* shows the kinematic limit. The $\theta_{\mathrm{jet}} = 0.12\,\mathrm{rad}$ shows the selection cut for jets

ponds roughly to the acceptance of the BCAL. The lower x edge of the bin for zero-jet events, x_{edge}, was determined from the condition $\theta_{\mathrm{jet}} > 0.12\,\mathrm{rad}$. For the bins where a jet was reconstructed, the bin widths in x were chosen to correspond to three times the resolution of the reconstructed x.

The MC simulation was used to study the x distribution of the zero-jet events. Figure 7 shows the true x distribution for the 99–00 e^+p MC events in different Q^2 bins. Similar distributions are observed in the 98–99 e^-p and 96–97 e^+p MC. As can be seen in this figure, the zero-jet events originate predominantly from the interval $x_{\mathrm{edge}} < x < 1$. We note that these distributions depend on the particular PDF chosen and that there are uncertainties at large x.

The efficiency, defined as the number of events generated and reconstructed in a bin after all selection cuts divided by the number of events that were generated in that bin, was typically 40%. In some low-Q^2 bins, dominated by events in which the electron is scattered into the RCAL or the B/RCAL transition region and removed by the fiducial cut, the efficiency was lower.

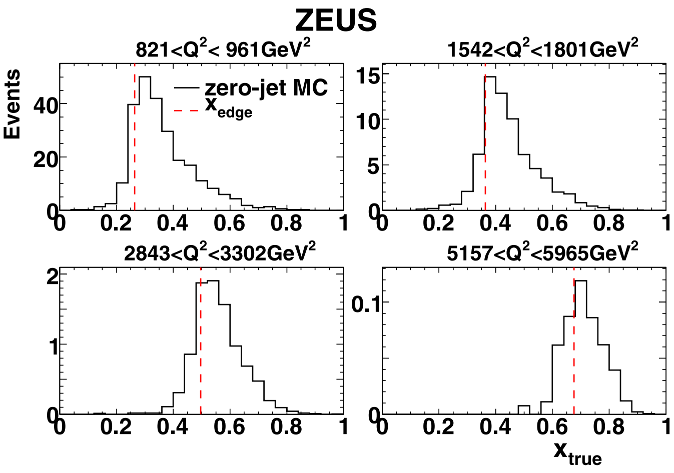

Fig. 7. The true x distribution for zero-jet events from 99–00 e^+p MC simulations in different Q^2 bins. The *dashed lines* represent the lower edge of the bins, x_{edge}. The MC distributions are normalized to the luminosity of the data

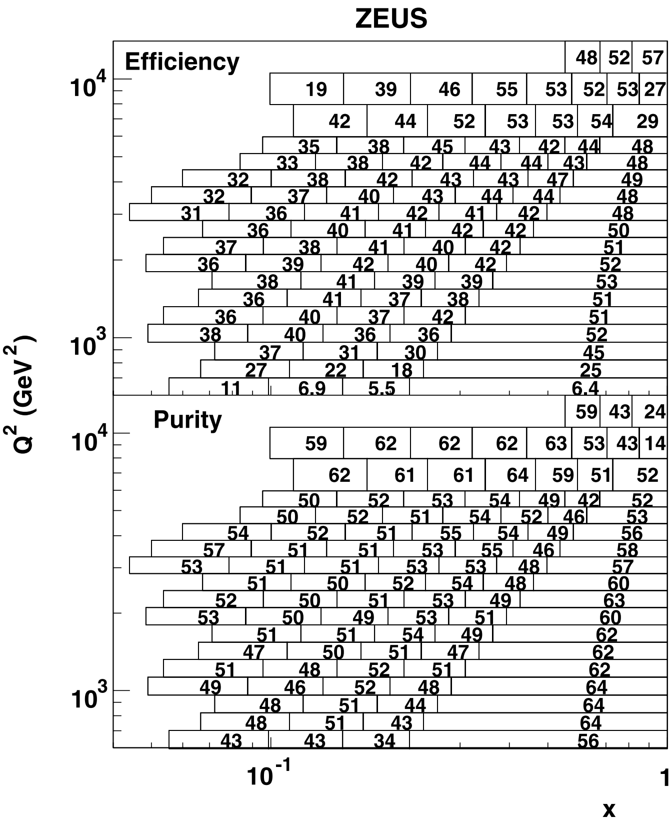

Fig. 8. The efficiency and purity in % for each bin are shown for 99–00 e^+p data

The purity, defined as the number of events generated and reconstructed in a bin after all selection cuts divided by the total number of events reconstructed in that bin, was typically 50%. The efficiency and purity in the (x, Q^2) bins for the 99–00 e^+p simulation are shown in Fig. 8. The 96–97 e^+p and 98–99 e^-p simulations yielded similar values. The efficiency and purity in zero-jet bins are comparable to those in the mid-x bins.

The double-differential cross section was determined as

$$\frac{\mathrm{d}^2\sigma_{\mathrm{Born}}\left(x,Q^2\right)}{\mathrm{d}x\mathrm{d}Q^2}=\frac{N_{\mathrm{data}}\left(\Delta x,\Delta Q^2\right)}{N_{\mathrm{MC}}\left(\Delta x,\Delta Q^2\right)}\left(1+\delta\left(Q^2\right)\right)\times\frac{\mathrm{d}^2\sigma^{\mathrm{SM}}_{\mathrm{Born}}}{\mathrm{d}x\mathrm{d}Q^2}\,,$$

and the integrated cross section was determined as

$$\int_{x_{\mathrm{edge}}}^{1}\frac{\mathrm{d}^2\sigma_{\mathrm{Born}}\left(x,Q^2\right)}{\mathrm{d}x\mathrm{d}Q^2}\mathrm{d}x=\frac{N_{\mathrm{data}}\left(\Delta x,\Delta Q^2\right)}{N_{\mathrm{MC}}\left(\Delta x,\Delta Q^2\right)}\left(1+\delta\left(Q^2\right)\right)\times\int_{x_{\mathrm{edge}}}^{1}\frac{\mathrm{d}^2\sigma^{\mathrm{SM}}_{\mathrm{Born}}}{\mathrm{d}x\mathrm{d}Q^2}\mathrm{d}x\,,$$

where $N_{\mathrm{data}}(\Delta x,\Delta Q^2)$ is the number of data events in a bin $(\Delta x,\Delta Q^2)$ and $N_{\mathrm{MC}}(\Delta x,\Delta Q^2)$ is the number of signal MC events normalized to the luminosity of the data. The SM prediction, $\mathrm{d}^2\sigma^{\mathrm{SM}}_{\mathrm{Born}}(x,Q^2)/\mathrm{d}x\mathrm{d}Q^2$, was evaluated according to (1) with the same PDF and electroweak (EW) parameters as used in the MC simulation. This procedure implicitly takes the acceptance, bin-centering and leading-order radiative corrections from the MC simulation. The variation of the cross sections resulting from different choices of PDF in the MC are described in the next section. The values of (x,Q^2) at which the cross sections are quoted are given in Tables 1–6.

Monte Carlo studies indicated that the radiative corrections have little dependence on x for the kinematic reconstruction method used here. The correction for higher-order radiative effects, $\delta(Q^2)$, calculated from HECTOR [38] varied from 3% at low Q^2 to 0% at high Q^2.

Table 1. The cross-section table for 96–97 e^+p NC scattering. The first two columns of the table contain the Q^2 and x values at which the cross section is quoted, the third contains the measured cross section $\mathrm{d}^2\sigma/\mathrm{d}x\mathrm{d}Q^2$ corrected to the electroweak Born level or the upper limit in case of zero observed events, the fourth contains the number of events reconstructed in the bin, N, the fifth contains the statistical uncertainty, δ_s, and the sixth contains the total systematic uncertainty, δ_t. The right part of the table lists the total uncorrelated systematic uncertainty, δ_u, followed by the bin-to-bin correlated systematic uncertainties δ_1–δ_6 defined in the text. The upper (lower) numbers refer to the variation of the cross section, whereas the signs of the numbers reflect the direction of change in the cross sections. Note that the normalization uncertainty, δ_7, is not listed

Q^2 (GeV^2)	x	$\mathrm{d}^2\sigma/\mathrm{d}x\mathrm{d}Q^2$ (pb/GeV^2)	N	δ_s (%)	δ_t (%)	δ_u (%)	δ_1 (%)	δ_2 (%)	δ_3 (%)	δ_4 (%)	δ_5 (%)	δ_6 (%)
648	0.09	2.66	114	$^{+10}_{-8.5}$	$^{+7.3}_{-7.1}$	$^{+2.0}_{-1.6}$	$^{+6.0}_{-6.1}$	$^{-0.3}_{+1.2}$	$^{-0.2}_{+0.1}$	$^{+1.4}_{-1.4}$	$^{+2.4}_{-2.4}$	$^{+0.8}_{-0.8}$
	0.15	1.08	40	$^{+18}_{-13}$	$^{+7.7}_{-8.2}$	$^{+2.1}_{-2.2}$	$^{+6.4}_{-6.7}$	$^{-1.3}_{+0.4}$	$^{+1.6}_{-2.1}$	$^{+0.9}_{-0.9}$	$^{+2.4}_{-2.4}$	$^{+1.5}_{-1.5}$
	0.21	$7.97\cdot10^{-1}$	33	$^{+20}_{-15}$	$^{+11}_{-9.1}$	$^{+3.6}_{-2.0}$	$^{+9.2}_{-8.1}$	$^{-0.4}_{+2.5}$	$^{+2.7}_{-0.2}$	$^{+0.5}_{-0.5}$	$^{+2.4}_{-2.4}$	$^{+2.2}_{-2.2}$
761	0.06	3.06	299	$^{+6.1}_{-5.4}$	$^{+3.8}_{-3.5}$	$^{+1.3}_{-0.7}$	$^{+1.0}_{-0.6}$	$^{-0.4}_{-0.1}$	$^{-0.4}_{+0.2}$	$^{+1.7}_{-1.7}$	$^{+2.4}_{-2.4}$	$^{+0.5}_{-0.5}$
	0.11	1.72	187	$^{+7.9}_{-6.8}$	$^{+4.3}_{-4.7}$	$^{+0.2}_{-1.0}$	$^{+2.4}_{-3.0}$	$^{-0.9}_{+1.5}$	$^{-0.0}_{-0.3}$	$^{+1.3}_{-1.3}$	$^{+2.4}_{-2.4}$	$^{+1.0}_{-1.0}$
	0.16	$8.11\cdot10^{-1}$	92	$^{+12}_{-9.4}$	$^{+5.5}_{-7.7}$	$^{+0.8}_{-2.1}$	$^{+4.2}_{-6.1}$	$^{-1.4}_{-0.3}$	$^{+0.3}_{-2.0}$	$^{+0.8}_{-0.8}$	$^{+2.4}_{-2.4}$	$^{+1.6}_{-1.6}$
	0.23	$6.09\cdot10^{-1}$	88	$^{+12}_{-9.6}$	$^{+7.0}_{-5.0}$	$^{+0.9}_{-1.5}$	$^{+4.8}_{-2.8}$	$^{-0.6}_{+2.6}$	$^{+1.9}_{+0.5}$	$^{+0.6}_{-0.6}$	$^{+2.4}_{-2.4}$	$^{+2.4}_{-2.4}$
891	0.07	1.89	314	$^{+6.0}_{-5.4}$	$^{+3.6}_{-3.5}$	$^{+1.0}_{-0.3}$	$^{-0.8}_{+0.8}$	$^{-0.3}_{+0.3}$	$^{-0.3}_{+0.3}$	$^{+1.6}_{-1.6}$	$^{+2.4}_{-2.4}$	$^{+0.6}_{-0.6}$
	0.12	$9.96\cdot10^{-1}$	214	$^{+7.3}_{-6.4}$	$^{+3.7}_{-3.5}$	$^{+1.2}_{-0.6}$	$^{+1.1}_{+0.2}$	$^{-0.9}_{+0.2}$	$^{+0.0}_{-0.3}$	$^{+1.2}_{-1.2}$	$^{+2.4}_{-2.4}$	$^{+1.1}_{-1.1}$
	0.18	$5.96\cdot10^{-1}$	145	$^{+9.1}_{-7.6}$	$^{+4.0}_{-3.9}$	$^{+1.4}_{-0.8}$	$^{+0.4}_{+0.4}$	$^{-1.1}_{+0.9}$	$^{+0.9}_{-1.1}$	$^{+0.7}_{-0.7}$	$^{+2.4}_{-2.4}$	$^{+1.8}_{-1.8}$
	0.25	$2.92\cdot10^{-1}$	91	$^{+12}_{-9.4}$	$^{+4.7}_{-5.8}$	$^{+0.7}_{-1.1}$	$^{+0.5}_{-3.0}$	$^{-1.9}_{+1.5}$	$^{+1.6}_{-2.0}$	$^{+0.8}_{-0.8}$	$^{+2.4}_{-2.4}$	$^{+2.6}_{-2.6}$
1045	0.08	1.16	251	$^{+6.8}_{-5.9}$	$^{+3.6}_{-3.6}$	$^{+0.6}_{-0.4}$	$^{-1.2}_{+1.0}$	$^{-0.5}_{+0.2}$	$^{-0.2}_{+0.5}$	$^{+1.6}_{-1.6}$	$^{+2.4}_{-2.4}$	$^{+0.7}_{-0.7}$
	0.13	$6.10\cdot10^{-1}$	182	$^{+8.0}_{-6.9}$	$^{+3.5}_{-3.8}$	$^{+0.7}_{-1.1}$	$^{-0.8}_{+0.2}$	$^{-1.0}_{+0.8}$	$^{-0.2}_{-0.3}$	$^{+1.1}_{-1.1}$	$^{+2.4}_{-2.4}$	$^{+1.2}_{-1.2}$
	0.19	$3.79\cdot10^{-1}$	143	$^{+9.1}_{-7.7}$	$^{+4.8}_{-4.2}$	$^{+1.3}_{-0.8}$	$^{-1.7}_{+2.1}$	$^{+0.2}_{+0.7}$	$^{+1.9}_{-1.2}$	$^{+0.6}_{-0.6}$	$^{+2.4}_{-2.4}$	$^{+1.9}_{-1.9}$
	0.27	$1.94\cdot10^{-1}$	94	$^{+11}_{-9.3}$	$^{+5.2}_{-5.2}$	$^{+2.0}_{-0.5}$	$^{-0.3}_{+1.1}$	$^{-2.9}_{+1.8}$	$^{+1.0}_{-1.0}$	$^{+0.9}_{-0.9}$	$^{+2.4}_{-2.4}$	$^{+2.9}_{-2.9}$
1224	0.09	$7.98\cdot10^{-1}$	233	$^{+7.0}_{-6.2}$	$^{+3.6}_{-3.8}$	$^{+0.0}_{-0.7}$	$^{-1.6}_{+1.3}$	$^{-0.2}_{-0.0}$	$^{-0.5}_{+0.3}$	$^{+1.6}_{-1.6}$	$^{+2.4}_{-2.4}$	$^{+0.8}_{-0.8}$
	0.14	$4.26\cdot10^{-1}$	169	$^{+8.3}_{-7.2}$	$^{+4.2}_{-3.6}$	$^{+1.0}_{-0.4}$	$^{-0.4}_{+2.2}$	$^{-1.1}_{+0.9}$	$^{+0.1}_{-0.4}$	$^{+0.9}_{-0.9}$	$^{+2.4}_{-2.4}$	$^{+1.3}_{-1.3}$
	0.21	$2.04\cdot10^{-1}$	91	$^{+12}_{-9.4}$	$^{+4.3}_{-4.3}$	$^{+1.8}_{-0.4}$	$^{+1.0}_{+0.2}$	$^{-0.4}_{-0.6}$	$^{+1.1}_{-2.2}$	$^{+0.6}_{-0.6}$	$^{+2.4}_{-2.4}$	$^{+2.2}_{-2.2}$
	0.30	$1.25\cdot10^{-1}$	78	$^{+13}_{-10}$	$^{+5.7}_{-5.2}$	$^{+0.6}_{-1.7}$	$^{-1.7}_{+0.6}$	$^{-0.7}_{+2.7}$	$^{+1.8}_{-0.1}$	$^{+1.1}_{-1.1}$	$^{+2.4}_{-2.4}$	$^{+3.3}_{-3.3}$
1431	0.06	$7.68\cdot10^{-1}$	170	$^{+8.3}_{-7.1}$	$^{+3.9}_{-3.8}$	$^{+1.0}_{-0.5}$	$^{-1.1}_{+1.4}$	$^{-0.8}_{-0.3}$	$^{-0.2}_{-0.4}$	$^{+1.8}_{-1.8}$	$^{+2.4}_{-2.4}$	$^{+0.5}_{-0.5}$
	0.10	$3.83\cdot10^{-1}$	126	$^{+9.7}_{-8.1}$	$^{+4.0}_{-3.7}$	$^{+1.0}_{-1.2}$	$^{-0.7}_{+1.6}$	$^{+1.0}_{+0.4}$	$^{-0.1}_{+0.5}$	$^{+1.5}_{-1.5}$	$^{+2.4}_{-2.4}$	$^{+0.9}_{-0.9}$
	0.16	$2.27\cdot10^{-1}$	112	$^{+10}_{-8.6}$	$^{+3.6}_{-4.0}$	$^{+0.5}_{-0.3}$	$^{-1.0}_{+0.5}$	$^{-1.8}_{+0.8}$	$^{-0.2}_{-0.6}$	$^{+0.8}_{-0.8}$	$^{+2.4}_{-2.4}$	$^{+1.6}_{-1.6}$
	0.23	$1.19\cdot10^{-1}$	70	$^{+13}_{-10}$	$^{+4.8}_{-4.2}$	$^{+1.9}_{-0.9}$	$^{-1.0}_{+2.0}$	$^{-0.0}_{-0.2}$	$^{+1.1}_{-1.3}$	$^{+0.7}_{-0.7}$	$^{+2.4}_{-2.4}$	$^{+2.4}_{-2.4}$
	0.32	$7.17\cdot10^{-2}$	59	$^{+15}_{-12}$	$^{+5.7}_{-5.3}$	$^{+0.8}_{-0.4}$	$^{-0.3}_{+0.6}$	$^{-2.0}_{+2.3}$	$^{+1.8}_{-1.1}$	$^{+1.4}_{-1.4}$	$^{+2.4}_{-2.4}$	$^{+3.6}_{-3.6}$

Table 1. Continued

Q^2 (GeV^2)	x	$\mathrm{d}^2\sigma/\mathrm{d}x\mathrm{d}Q^2$ (pb/GeV^2)	N	δ_s (%)	δ_t (%)	δ_u (%)	δ_1 (%)	δ_2 (%)	δ_3 (%)	δ_4 (%)	δ_5 (%)	δ_6 (%)
1672	0.07	$4.21\cdot 10^{-1}$	126	$^{+9.7}_{-8.1}$	$^{+4.3}_{-3.9}$	$^{+1.6}_{-0.5}$	$^{-1.6}_{+1.9}$	$^{-0.1}_{+0.1}$	$^{-0.1}_{-0.1}$	$^{+1.8}_{-1.8}$	$^{+2.4}_{-2.4}$	$^{+0.6}_{-0.6}$
	0.11	$3.25\cdot 10^{-1}$	144	$^{+9.1}_{-7.7}$	$^{+4.0}_{-4.0}$	$^{+0.6}_{-0.7}$	$^{-2.0}_{+2.0}$	$^{-0.3}_{+0.3}$	$^{-0.3}_{+0.1}$	$^{+1.3}_{-1.3}$	$^{+2.4}_{-2.4}$	$^{+1.0}_{-1.0}$
	0.17	$1.35\cdot 10^{-1}$	80	$^{+12}_{-10}$	$^{+3.5}_{-4.0}$	$^{+0.4}_{-1.4}$	$^{-1.3}_{-0.2}$	$^{-0.8}_{+0.5}$	$^{+0.2}_{-0.1}$	$^{+0.7}_{-0.7}$	$^{+2.4}_{-2.4}$	$^{+1.7}_{-1.7}$
	0.25	$7.96\cdot 10^{-2}$	55	$^{+15}_{-12}$	$^{+4.1}_{-5.4}$	$^{+0.3}_{-2.4}$	$^{-2.0}_{-0.1}$	$^{-1.5}_{+0.6}$	$^{+0.6}_{-1.2}$	$^{+0.8}_{-0.8}$	$^{+2.4}_{-2.4}$	$^{+2.6}_{-2.6}$
	0.35	$4.27\cdot 10^{-2}$	45	$^{+17}_{-13}$	$^{+7.5}_{-6.2}$	$^{+4.1}_{-1.0}$	$^{-1.7}_{+1.5}$	$^{-2.1}_{+2.7}$	$^{+1.5}_{-1.5}$	$^{+1.8}_{-1.8}$	$^{+2.4}_{-2.4}$	$^{+4.0}_{-4.0}$
1951	0.08	$3.32\cdot 10^{-1}$	130	$^{+9.6}_{-8.1}$	$^{+3.8}_{-4.4}$	$^{+0.5}_{-1.5}$	$^{-2.2}_{+1.2}$	$^{-0.5}_{+0.6}$	$^{-0.1}_{-0.1}$	$^{+1.8}_{-1.8}$	$^{+2.4}_{-2.4}$	$^{+0.7}_{-0.7}$
	0.13	$1.66\cdot 10^{-1}$	86	$^{+12}_{-9.7}$	$^{+3.6}_{-3.8}$	$^{+0.9}_{-0.9}$	$^{-1.2}_{+1.1}$	$^{-0.6}_{-0.6}$	$^{-0.3}_{+0.1}$	$^{+1.2}_{-1.2}$	$^{+2.4}_{-2.4}$	$^{+1.2}_{-1.2}$
	0.19	$8.47\cdot 10^{-2}$	66	$^{+14}_{-11}$	$^{+4.6}_{-4.2}$	$^{+0.9}_{-1.4}$	$^{-1.6}_{+2.6}$	$^{-0.7}_{+0.9}$	$^{+0.1}_{-0.2}$	$^{+0.7}_{-0.7}$	$^{+2.4}_{-2.4}$	$^{+1.9}_{-1.9}$
	0.27	$4.53\cdot 10^{-2}$	41	$^{+18}_{-13}$	$^{+5.0}_{-4.3}$	$^{+1.6}_{-0.4}$	$^{-0.3}_{+1.9}$	$^{-0.6}_{+0.8}$	$^{+0.9}_{-0.6}$	$^{+1.0}_{-1.0}$	$^{+2.4}_{-2.4}$	$^{+2.9}_{-2.9}$
	0.38	$2.69\cdot 10^{-2}$	35	$^{+20}_{-14}$	$^{+6.5}_{-6.5}$	$^{+0.3}_{-1.4}$	$^{-1.3}_{-0.3}$	$^{-1.8}_{+2.4}$	$^{+1.8}_{-1.4}$	$^{+2.2}_{-2.2}$	$^{+2.4}_{-2.4}$	$^{+4.5}_{-4.5}$
2273	0.09	$1.88\cdot 10^{-1}$	88	$^{+12}_{-9.6}$	$^{+3.6}_{-4.3}$	$^{+0.3}_{-1.5}$	$^{-2.0}_{+1.1}$	$^{-0.9}_{+0.4}$	$^{-0.4}_{-0.0}$	$^{+1.7}_{-1.7}$	$^{+2.4}_{-2.4}$	$^{+0.8}_{-0.8}$
	0.14	$8.43\cdot 10^{-2}$	60	$^{+15}_{-11}$	$^{+4.1}_{-4.0}$	$^{+0.4}_{-0.7}$	$^{-2.1}_{+2.1}$	$^{+0.8}_{-0.5}$	$^{-0.2}_{+0.2}$	$^{+1.0}_{-1.0}$	$^{+2.4}_{-2.4}$	$^{+1.3}_{-1.3}$
	0.21	$6.76\cdot 10^{-2}$	59	$^{+15}_{-12}$	$^{+4.0}_{-4.4}$	$^{+0.4}_{-1.0}$	$^{-0.9}_{+0.1}$	$^{-1.9}_{+1.4}$	$^{+0.1}_{-0.4}$	$^{+0.7}_{-0.7}$	$^{+2.4}_{-2.4}$	$^{+2.2}_{-2.2}$
	0.30	$3.05\cdot 10^{-2}$	37	$^{+19}_{-14}$	$^{+5.1}_{-4.9}$	$^{+1.4}_{-0.7}$	$^{-0.3}_{+0.9}$	$^{-1.3}_{+1.3}$	$^{+0.6}_{-1.1}$	$^{+1.2}_{-1.2}$	$^{+2.4}_{-2.4}$	$^{+3.3}_{-3.3}$
	0.41	$1.56\cdot 10^{-2}$	25	$^{+24}_{-16}$	$^{+8.0}_{-6.6}$	$^{+2.2}_{-0.7}$	$^{+1.4}_{+1.0}$	$^{-1.8}_{+2.6}$	$^{+3.1}_{-0.5}$	$^{+2.7}_{-2.7}$	$^{+2.4}_{-2.4}$	$^{+4.9}_{-4.9}$
2644	0.06	$1.78\cdot 10^{-1}$	71	$^{+13}_{-11}$	$^{+4.4}_{-4.4}$	$^{+0.5}_{-1.3}$	$^{-2.1}_{+2.5}$	$^{-0.5}_{+0.0}$	$^{-0.1}_{-0.6}$	$^{+2.0}_{-2.0}$	$^{+2.4}_{-2.4}$	$^{+0.5}_{-0.5}$
	0.11	$9.53\cdot 10^{-2}$	53	$^{+16}_{-12}$	$^{+3.6}_{-3.7}$	$^{+0.6}_{-0.7}$	$^{-1.2}_{+0.4}$	$^{+0.0}_{+0.7}$	$^{-0.2}_{+0.1}$	$^{+1.6}_{-1.6}$	$^{+2.4}_{-2.4}$	$^{+1.0}_{-1.0}$
	0.16	$6.08\cdot 10^{-2}$	53	$^{+16}_{-12}$	$^{+4.0}_{-3.8}$	$^{+0.8}_{-0.5}$	$^{-1.5}_{+1.8}$	$^{-0.6}_{+0.5}$	$^{-0.4}_{-0.1}$	$^{+0.9}_{-0.9}$	$^{+2.4}_{-2.4}$	$^{+1.6}_{-1.6}$
	0.23	$3.70\cdot 10^{-2}$	41	$^{+18}_{-13}$	$^{+4.0}_{-4.2}$	$^{+0.7}_{-0.7}$	$^{-0.6}_{+0.6}$	$^{-1.6}_{+0.7}$	$^{+0.3}_{-0.4}$	$^{+0.7}_{-0.7}$	$^{+2.4}_{-2.4}$	$^{+2.4}_{-2.4}$
	0.33	$1.54\cdot 10^{-2}$	24	$^{+25}_{-16}$	$^{+6.7}_{-6.1}$	$^{+3.9}_{-1.9}$	$^{-2.3}_{+1.1}$	$^{-0.5}_{+1.2}$	$^{+1.4}_{-1.7}$	$^{+1.6}_{-1.6}$	$^{+2.4}_{-2.4}$	$^{+3.7}_{-3.7}$
	0.45	$7.21\cdot 10^{-3}$	13	$^{+36}_{-21}$	$^{+7.7}_{-9.2}$	$^{+0.8}_{-3.0}$	$^{-2.5}_{+0.6}$	$^{-4.4}_{+2.5}$	$^{-0.3}_{+1.2}$	$^{+3.3}_{-3.3}$	$^{+2.4}_{-2.4}$	$^{+5.6}_{-5.6}$
3073	0.07	$9.55\cdot 10^{-2}$	51	$^{+16}_{-12}$	$^{+4.5}_{-4.1}$	$^{+1.7}_{-1.6}$	$^{-1.1}_{+2.1}$	$^{-0.1}_{-0.1}$	$^{+0.1}_{-0.5}$	$^{+2.0}_{-2.0}$	$^{+2.4}_{-2.4}$	$^{+0.6}_{-0.6}$
	0.12	$6.15\cdot 10^{-2}$	42	$^{+18}_{-13}$	$^{+4.1}_{-4.3}$	$^{+1.9}_{-1.4}$	$^{-2.0}_{+1.0}$	$^{-1.0}_{+0.6}$	$^{-0.6}_{+0.0}$	$^{+1.4}_{-1.4}$	$^{+2.4}_{-2.4}$	$^{+1.1}_{-1.1}$
	0.18	$3.67\cdot 10^{-2}$	40	$^{+18}_{-13}$	$^{+4.0}_{-4.4}$	$^{+0.6}_{-0.9}$	$^{-2.4}_{+2.0}$	$^{-0.4}_{-0.8}$	$^{-0.2}_{-0.1}$	$^{+0.8}_{-0.8}$	$^{+2.4}_{-2.4}$	$^{+1.8}_{-1.8}$
	0.26	$2.30\cdot 10^{-2}$	31	$^{+21}_{-15}$	$^{+4.8}_{-4.7}$	$^{+0.6}_{-0.6}$	$^{-1.2}_{+0.6}$	$^{-1.8}_{+2.3}$	$^{+0.3}_{+0.2}$	$^{+0.9}_{-0.9}$	$^{+2.4}_{-2.4}$	$^{+2.8}_{-2.8}$
	0.36	$1.25\cdot 10^{-2}$	24	$^{+25}_{-16}$	$^{+6.0}_{-5.9}$	$^{+0.7}_{-0.8}$	$^{-1.1}_{+0.6}$	$^{-1.4}_{+2.1}$	$^{+1.0}_{-0.9}$	$^{+2.1}_{-2.1}$	$^{+2.4}_{-2.4}$	$^{+4.2}_{-4.2}$
	0.49	$5.38\cdot 10^{-3}$	13	$^{+36}_{-21}$	$^{+8.5}_{-9.1}$	$^{+0.7}_{-1.3}$	$^{+0.6}_{-0.5}$	$^{-4.0}_{+3.2}$	$^{-0.2}_{-1.9}$	$^{+3.8}_{-3.8}$	$^{+2.4}_{-2.4}$	$^{+6.2}_{-6.2}$
3568	0.09	$5.61\cdot 10^{-2}$	39	$^{+19}_{-14}$	$^{+4.8}_{-4.1}$	$^{+2.3}_{-0.7}$	$^{-1.7}_{+2.2}$	$^{+0.4}_{+0.7}$	$^{+0.3}_{-0.8}$	$^{+1.9}_{-1.9}$	$^{+2.4}_{-2.4}$	$^{+0.8}_{-0.8}$
	0.14	$2.97\cdot 10^{-2}$	27	$^{+23}_{-16}$	$^{+3.9}_{-5.4}$	$^{+0.6}_{-3.5}$	$^{-1.2}_{+1.6}$	$^{-1.8}_{+0.7}$	$^{-0.6}_{+0.7}$	$^{+1.1}_{-1.1}$	$^{+2.4}_{-2.4}$	$^{+1.3}_{-1.3}$
	0.21	$1.67\cdot 10^{-2}$	22	$^{+26}_{-17}$	$^{+4.2}_{-3.9}$	$^{+0.7}_{-0.7}$	$^{-1.1}_{+1.8}$	$^{-0.1}_{+0.7}$	$^{-0.1}_{-0.1}$	$^{+0.7}_{-0.7}$	$^{+2.4}_{-2.4}$	$^{+2.2}_{-2.2}$
	0.29	$1.04\cdot 10^{-2}$	19	$^{+29}_{-18}$	$^{+5.2}_{-4.6}$	$^{+1.1}_{-0.4}$	$^{+0.6}_{+1.9}$	$^{-0.9}_{+1.3}$	$^{+0.1}_{-0.3}$	$^{+1.2}_{-1.2}$	$^{+2.4}_{-2.4}$	$^{+3.2}_{-3.2}$
	0.40	$6.43\cdot 10^{-3}$	16	$^{+32}_{-19}$	$^{+7.7}_{-6.9}$	$^{+1.3}_{-0.1}$	$^{-1.2}_{+4.1}$	$^{-2.7}_{+1.6}$	$^{+0.8}_{-1.0}$	$^{+2.6}_{-2.6}$	$^{+2.4}_{-2.4}$	$^{+4.8}_{-4.8}$
	0.53	$1.37\cdot 10^{-3}$	4	$^{+78}_{-29}$	$^{+10}_{-9.8}$	$^{+1.5}_{-0.6}$	$^{-0.2}_{+1.6}$	$^{-4.6}_{+4.5}$	$^{+0.8}_{-0.3}$	$^{+4.3}_{-4.3}$	$^{+2.4}_{-2.4}$	$^{+6.9}_{-6.9}$
4145	0.10	$3.18\cdot 10^{-2}$	26	$^{+24}_{-16}$	$^{+4.1}_{-5.7}$	$^{+0.4}_{-3.5}$	$^{-2.6}_{+2.2}$	$^{-1.0}_{+0.2}$	$^{+0.2}_{-0.5}$	$^{+1.7}_{-1.7}$	$^{+2.4}_{-2.4}$	$^{+0.9}_{-0.9}$
	0.16	$2.61\cdot 10^{-2}$	32	$^{+21}_{-15}$	$^{+4.9}_{-4.4}$	$^{+3.1}_{-1.0}$	$^{-2.5}_{+1.5}$	$^{-0.3}_{+0.5}$	$^{-0.4}_{+0.3}$	$^{+0.9}_{-0.9}$	$^{+2.4}_{-2.4}$	$^{+1.6}_{-1.6}$
	0.23	$7.72\cdot 10^{-3}$	14	$^{+35}_{-20}$	$^{+7.9}_{-4.9}$	$^{+6.8}_{-1.1}$	$^{-2.5}_{+0.7}$	$^{-1.3}_{+1.3}$	$^{-0.2}_{-0.4}$	$^{+0.7}_{-0.7}$	$^{+2.4}_{-2.4}$	$^{+2.4}_{-2.4}$
	0.33	$8.50\cdot 10^{-3}$	20	$^{+28}_{-18}$	$^{+5.6}_{-5.9}$	$^{+0.7}_{-1.1}$	$^{-2.3}_{+1.8}$	$^{-1.7}_{+1.5}$	$^{+0.4}_{+0.3}$	$^{+1.6}_{-1.6}$	$^{+2.4}_{-2.4}$	$^{+3.7}_{-3.7}$
	0.44	$3.03\cdot 10^{-3}$	9	$^{+46}_{-24}$	$^{+7.0}_{-14}$	$^{+0.0}_{-11}$	$^{-1.6}_{-0.7}$	$^{-4.0}_{+1.0}$	$^{+0.5}_{-2.1}$	$^{+3.3}_{-3.3}$	$^{+2.4}_{-2.4}$	$^{+5.4}_{-5.4}$
	0.58	$2.96\cdot 10^{-4}$	1	$^{+220}_{-30}$	$^{+13}_{-10}$	$^{+1.3}_{-2.4}$	$^{+0.0}_{-2.0}$	$^{-2.6}_{+7.7}$	$^{-0.9}_{+4.4}$	$^{+4.7}_{-4.7}$	$^{+2.4}_{-2.4}$	$^{+7.8}_{-7.8}$

Table 1. Continued

Q^2 (GeV^2)	x	$\mathrm{d}^2\sigma/\mathrm{d}x\mathrm{d}Q^2$ (pb/GeV^2)	N	δ_s (%)	δ_t (%)	δ_u (%)	δ_1 (%)	δ_2 (%)	δ_3 (%)	δ_4 (%)	δ_5 (%)	δ_6 (%)
4806	0.12	$1.76 \cdot 10^{-2}$	18	+30 −18	+3.8 −6.3	+0.6 −5.0	−1.6 +1.3	+0.4 −0.4	+0.3 −0.3	+1.5 −1.5	+2.4 −2.4	+1.1 −1.1
	0.18	$1.36 \cdot 10^{-2}$	20	+28 −18	+4.4 −4.0	+1.1 −0.6	−0.4 +1.2	−1.6 +2.2	−0.9 +0.3	+0.7 −0.7	+2.4 −2.4	+1.8 −1.8
	0.26	$5.44 \cdot 10^{-3}$	12	+38 −21	+4.5 −4.5	+0.6 −0.8	−0.8 +1.6	−1.4 +0.8	+0.1 +0.0	+0.9 −0.9	+2.4 −2.4	+2.8 −2.8
	0.36	$3.48 \cdot 10^{-3}$	10	+43 −23	+6.5 −6.1	+1.6 −0.5	−1.2 +2.8	−2.1 +1.3	−0.2 −0.7	+2.1 −2.1	+2.4 −2.4	+4.2 −4.2
	0.49	$1.12 \cdot 10^{-3}$	4	+78 −29	+9.4 −8.6	+1.8 −0.6	−1.6 +2.8	−2.8 +3.9	+1.0 −0.5	+3.9 −3.9	+2.4 −2.4	+6.2 −6.2
	0.63	$9.18 \cdot 10^{-4}$	4	+78 −29	+15 −12	+1.0 −2.0	−2.3 −0.3	−4.8 +9.6	−1.0 +4.8	+4.9 −4.9	+2.4 −2.4	+8.8 −8.8
5561	0.09	$2.26 \cdot 10^{-2}$	15	+33 −20	+6.1 −9.1	+1.8 −6.5	−4.1 +3.5	+3.1 −3.1	−0.1 −0.5	+1.9 −1.9	+2.4 −2.4	+0.8 −0.8
	0.14	$1.42 \cdot 10^{-2}$	21	+27 −17	+4.3 −4.3	+0.7 −1.4	−2.2 +2.5	−0.3 +0.6	−0.1 −0.4	+1.1 −1.1	+2.4 −2.4	+1.3 −1.3
	0.21	$3.41 \cdot 10^{-3}$	6	+60 −26	+4.0 −4.6	+0.6 −0.9	−2.0 +1.5	−1.4 −0.3	−0.7 +0.3	+0.7 −0.7	+2.4 −2.4	+2.2 −2.2
	0.30	$4.92 \cdot 10^{-3}$	14	+35 −20	+5.3 −5.4	+0.4 −0.7	−2.4 +1.1	−1.7 +2.5	+0.1 −0.3	+1.2 −1.2	+2.4 −2.4	+3.3 −3.3
	0.41	$2.56 \cdot 10^{-3}$	9	+46 −24	+6.5 −7.1	+0.7 −1.5	−1.8 +0.0	−2.1 +1.0	+0.4 −0.2	+2.8 −2.8	+2.4 −2.4	+4.9 −4.9
	0.54	$9.13 \cdot 10^{-4}$	4	+78 −29	+10 −10	+0.4 −2.2	−1.8 −0.1	−4.2 +5.1	−0.3 −1.1	+4.6 −4.6	+2.4 −2.4	+7.1 −7.1
	0.69	$6.11 \cdot 10^{-4}$	3	+96 −30	+16 −14	+5.8 −2.1	+0.3 +1.8	−7.3 +9.2	−3.1 +3.1	+4.6 −4.6	+2.4 −2.4	+10 −10
6966	0.11	$6.88 \cdot 10^{-3}$	13	+36 −21	+5.5 −9.4	+0.4 −6.6	−4.2 +2.3	+3.5 −3.6	−0.1 −1.5	+1.8 −1.8	+2.4 −2.4	+1.0 −1.0
	0.17	$6.24 \cdot 10^{-3}$	25	+24 −16	+3.8 −7.2	+0.0 −5.3	−2.9 +1.7	−2.0 +0.3	−0.6 −0.2	+0.8 −0.8	+2.4 −2.4	+1.7 −1.7
	0.25	$2.85 \cdot 10^{-3}$	15	+33 −20	+4.5 −4.4	+0.6 −0.8	−1.6 +1.8	−0.4 +0.8	−0.5 +0.0	+0.7 −0.7	+2.4 −2.4	+2.6 −2.6
	0.34	$2.52 \cdot 10^{-3}$	22	+26 −17	+5.7 −5.7	+0.7 −0.8	−1.3 +1.9	−1.9 +1.3	+0.1 −0.1	+1.8 −1.8	+2.4 −2.4	+3.9 −3.9
	0.47	$6.97 \cdot 10^{-4}$	7	+54 −25	+8.8 −8.3	+1.1 −0.4	−0.7 +1.3	−3.3 +4.2	+0.3 −0.5	+3.7 −3.7	+2.4 −2.4	+5.9 −5.9
	0.61	$6.75 \cdot 10^{-4}$	8	+49 −24	+13 −13	+1.3 −0.6	−1.1 +3.0	−7.9 +6.6	−0.5 −0.1	+5.0 −5.0	+2.4 −2.4	+8.4 −8.4
	0.78	$< 4.42 \cdot 10^{-5}$	0									
9055	0.16	$5.35 \cdot 10^{-3}$	16	+32 −19	+5.8 −12	+0.4 −9.9	−4.6 +3.8	+2.6 −3.4	+0.6 −1.4	+1.0 −1.0	+2.4 −2.4	+1.6 −1.6
	0.23	$2.96 \cdot 10^{-3}$	17	+30 −19	+4.3 −5.3	+1.3 −1.7	−2.6 +1.2	−1.9 +1.2	−1.1 +0.3	+0.4 −0.4	+2.4 −2.4	+2.4 −2.4
	0.33	$1.23 \cdot 10^{-3}$	12	+38 −21	+5.4 −5.7	+0.6 −0.7	−2.2 +1.6	−1.7 +1.4	−0.3 −0.1	+1.5 −1.5	+2.4 −2.4	+3.7 −3.7
	0.45	$4.31 \cdot 10^{-4}$	5	+67 −28	+8.0 −8.4	+0.4 −0.7	−1.3 +0.4	−4.2 +3.4	+0.1 −0.3	+3.4 −3.4	+2.4 −2.4	+5.6 −5.6
	0.59	$2.12 \cdot 10^{-4}$	3	+96 −30	+12 −10	+0.6 −0.7	−1.4 −0.4	−2.3 +7.3	+0.1 +0.3	+5.1 −5.1	+2.4 −2.4	+8.0 −8.0
	0.73	$6.86 \cdot 10^{-5}$	1	+220 −30	+15 −27	+1.1 −6.2	−2.3 −2.5	−23 +8.3	−0.9 +2.2	+4.6 −4.6	+2.4 −2.4	+11 −11
	0.90	$< 8.12 \cdot 10^{-6}$	0									
14807	0.76	$1.03 \cdot 10^{-5}$	1	+220 −30	+18 −20	+2.1 −2.6	−2.7 +1.6	−15 +14	−1.5 +0.7	+2.5 −2.5	+2.4 −2.4	+12 −12
	0.92	$< 1.28 \cdot 10^{-6}$	0									

Table 2. The integral cross section table for 96–97 e^+p NC scattering. The first two columns of the table contain the Q^2 and x_{edge} values for the bin, the third contains the measured cross section $\int_{x_{\mathrm{edge}}}^{1} \mathrm{d}^2\sigma/\mathrm{d}x\mathrm{d}Q^2$ corrected to the electroweak Born level or the upper limit in case of zero observed events, the fourth contains the number of events reconstructed in the bin, N, the fifth contains the statistical uncertainty, δ_s, and the sixth contains the total systematic uncertainty, δ_t. The right part of the table lists the total uncorrelated systematic uncertainty, δ_u, followed by the bin-to-bin correlated systematic uncertainties δ_1–δ_6 defined in the text. The upper (lower) numbers refer to the variation of the cross section, whereas the signs of the numbers reflect the direction of change in the cross sections. Note that the normalization uncertainty, δ_7, is not listed

Q^2 (GeV^2)	x_{edge}	$\int_{x_{\mathrm{edge}}}^{1} \mathrm{d}^2\sigma/\mathrm{d}x\mathrm{d}Q^2$ (pb/GeV^2)	N	δ_s (%)	δ_t (%)	δ_u (%)	δ_1 (%)	δ_2 (%)	δ_3 (%)	δ_4 (%)	δ_5 (%)	δ_6 (%)
648	0.25	$8.49 \cdot 10^{-2}$	34	+20 −14	+9.5 −7.9	+4.9 −2.7	+6.1 −5.2	+0.6 +0.6	−0.8 +1.1	+2.0 −2.0	+1.6 −1.6	+4.3 −4.3
761	0.27	$4.66 \cdot 10^{-2}$	74	+13 −10	+6.9 −5.9	+1.8 −1.1	+3.0 −0.6	+0.9 +0.9	−0.7 +0.7	+2.5 −2.5	+1.6 −1.6	+4.6 −4.6
891	0.30	$3.19 \cdot 10^{-2}$	109	+10 −8.7	+8.1 −6.1	+4.6 −0.1	+2.2 +0.5	+1.1 +1.1	−1.0 +1.1	+2.7 −2.7	+1.6 −1.6	+4.9 −4.9

Table 2. Continued

Q^2 (GeV^2)	x_{edge}	$\int_{x_{\mathrm{edge}}}^{1} \mathrm{d}^2\sigma/\mathrm{d}x\mathrm{d}Q^2$ (pb/GeV^2)	N	δ_s (%)	δ_t (%)	δ_u (%)	δ_1 (%)	δ_2 (%)	δ_3 (%)	δ_4 (%)	δ_5 (%)	δ_6 (%)
1045	0.32	$2.08 \cdot 10^{-2}$	101	+11 −9.1	+8.7 −7.9	+3.8 −0.6	−4.4 +4.2	+0.9 +0.9	−1.0 +0.7	+2.9 −2.9	+1.6 −1.6	+5.3 −5.3
1224	0.35	$1.03 \cdot 10^{-2}$	65	+14 −11	+8.2 −6.8	+3.0 −0.2	+0.6 +3.2	+0.7 +0.7	−0.4 +0.7	+3.1 −3.1	+1.6 −1.6	+5.6 −5.6
1431	0.38	$5.65 \cdot 10^{-3}$	42	+18 −13	+9.3 −8.5	+2.3 −0.1	−4.3 +5.3	+0.8 +0.8	−1.1 +0.7	+3.4 −3.4	+1.6 −1.6	+6.0 −6.0
1672	0.41	$3.66 \cdot 10^{-3}$	29	+22 −15	+8.7 −7.9	+2.2 −0.2	−1.3 +2.8	+0.5 +0.5	−0.7 +1.5	+3.7 −3.7	+1.6 −1.6	+6.4 −6.4
1951	0.44	$2.07 \cdot 10^{-3}$	21	+27 −17	+9.7 −8.9	+2.3 −0.6	−2.5 +4.1	+0.6 +0.6	−1.1 +1.0	+4.1 −4.1	+1.6 −1.6	+7.0 −7.0
2273	0.48	$1.22 \cdot 10^{-3}$	13	+36 −21	+10 −11	+4.1 −1.1	−5.7 +2.9	+0.4 +0.4	−2.9 +0.9	+4.6 −4.6	+1.6 −1.6	+7.6 −7.6
2644	0.52	$2.87 \cdot 10^{-4}$	4	+78 −29	+12 −10	+2.2 −3.0	−2.1 +6.5	+0.5 +0.5	−2.3 +0.9	+4.7 −4.7	+1.6 −1.6	+8.1 −8.1
3073	0.56	$< 8.32 \cdot 10^{-5}$	0									
3568	0.60	$6.04 \cdot 10^{-5}$	1	+220 −30	+14 −13	+4.5 −3.1	−6.1 +6.1	+1.4 +1.4	−2.1 +3.7	+4.7 −4.7	+1.6 −1.6	+9.4 −9.4
4145	0.65	$< 5.30 \cdot 10^{-5}$	0									
4806	0.70	$< 5.79 \cdot 10^{-5}$	0									
5561	0.76	$< 3.87 \cdot 10^{-5}$	0									
6966	0.89	$< 1.61 \cdot 10^{-6}$	0									

Table 3. The cross section table for 98–99 e^-p NC scattering. The first two columns of the table contain the Q^2 and x values at which the cross section is quoted, the third contains the measured cross section $\mathrm{d}^2\sigma/\mathrm{d}x\mathrm{d}Q^2$ corrected to the electroweak Born level or the upper limit in case of zero observed events, the fourth contains the number of events reconstructed in the bin, N, the fifth contains the statistical uncertainty, δ_s, and the sixth contains the total systematic uncertainty, δ_t. The right part of the table lists the total uncorrelated systematic uncertainty, δ_u, followed by the bin-to-bin correlated systematic uncertainties δ_1–δ_6 defined in the text. The upper (lower) numbers refer to the variation of the cross section, whereas the signs of the numbers reflect the direction of change in the cross sections. Note that the normalization uncertainty, δ_7, is not listed

Q^2 (GeV^2)	x	$\mathrm{d}^2\sigma/\mathrm{d}x\mathrm{d}Q^2$ (pb/GeV^2)	N	δ_s (%)	δ_t (%)	δ_u (%)	δ_1 (%)	δ_2 (%)	δ_3 (%)	δ_4 (%)	δ_5 (%)	δ_6 (%)
648	0.08	2.76	51	+16 −12	+8.3 −9.0	+0.7 −0.4	−7.0 +5.6	−1.1 +1.1	−3.0 +3.6	+0.1 −0.1	+2.4 −2.4	+3.4 −3.4
	0.13	1.78	23	+25 −17	+9.1 −12	+3.6 −3.3	−8.4 +6.0	−1.3 +0.1	−6.1 +3.3	+0.0 −0.0	+2.4 −2.4	+3.4 −3.4
	0.19	$8.63 \cdot 10^{-1}$	14	+35 −20	+11 −15	+1.0 −9.2	−9.2 +8.8	−1.4 +1.3	−5.4 +4.3	+0.0 +0.0	+2.4 −2.4	+3.4 −3.4
761	0.09	1.71	92	+12 −9.4	+6.1 −5.8	+1.0 −1.4	−2.5 +3.6	−0.9 +0.8	−1.6 +1.2	+0.1 −0.1	+2.4 −2.4	+3.3 −3.3
	0.14	$8.70 \cdot 10^{-1}$	44	+17 −13	+6.5 −6.5	+1.1 −1.1	−4.3 +4.2	−0.4 +0.3	−0.7 +1.4	+0.1 −0.1	+2.4 −2.4	+3.3 −3.3
	0.21	$6.10 \cdot 10^{-1}$	38	+19 −14	+6.8 −6.7	+1.3 −1.1	−4.0 +2.8	−1.4 +2.8	−2.0 +2.8	+0.0 −0.0	+2.4 −2.4	+3.3 −3.3
891	0.10	1.36	137	+9.3 −7.9	+4.8 −4.7	+0.6 −0.2	+0.0 −0.4	−0.6 +1.2	−0.2 −0.1	+0.1 −0.1	+2.4 −2.4	+3.2 −3.2
	0.15	$6.16 \cdot 10^{-1}$	61	+15 −11	+5.0 −4.8	+0.5 −0.2	−0.2 +0.6	−1.4 +0.2	+0.0 +1.7	+0.1 −0.1	+2.4 −2.4	+3.2 −3.2
	0.22	$5.20 \cdot 10^{-1}$	68	+14 −11	+5.5 −5.3	+2.2 −2.2	−1.3 +1.7	+0.4 +1.2	−0.2 −0.2	+0.0 +0.0	+2.4 −2.4	+3.2 −3.2
1045	0.07	1.56	148	+9.0 −7.6	+4.9 −5.2	+0.1 −0.6	+1.9 −2.4	+0.2 +0.2	+0.8 −1.1	+0.0 −0.0	+2.4 −2.4	+2.9 −2.9
	0.11	$6.53 \cdot 10^{-1}$	84	+12 −9.7	+4.6 −4.6	+0.3 −0.4	+0.2 −0.2	−1.3 +1.3	+0.4 −0.6	+0.1 −0.1	+2.4 −2.4	+2.9 −2.9
	0.17	$4.61 \cdot 10^{-1}$	67	+14 −11	+4.6 −4.8	+1.0 −1.4	+1.0 −0.2	−0.1 −0.2	−0.6 −1.2	+0.1 −0.1	+2.4 −2.4	+2.9 −2.9
	0.24	$2.02 \cdot 10^{-1}$	43	+18 −13	+4.8 −5.4	+1.1 −0.9	+0.4 −2.5	−1.5 +1.4	−0.4 +0.1	+0.1 −0.1	+2.4 −2.4	+2.9 −2.9
1224	0.07	$7.47 \cdot 10^{-1}$	87	+12 −9.6	+4.7 −4.9	+0.3 −1.1	+1.4 −1.7	+0.0 −0.4	+0.6 −0.4	+0.0 −0.0	+2.4 −2.4	+2.9 −2.9
	0.12	$4.90 \cdot 10^{-1}$	80	+13 −10	+4.7 −4.7	+0.3 −0.3	+0.9 −1.5	−0.9 +1.3	+0.5 −0.1	+0.1 −0.1	+2.4 −2.4	+2.9 −2.9
	0.18	$3.83 \cdot 10^{-1}$	70	+13 −11	+4.8 −4.6	+1.5 −0.2	−0.5 −1.0	−0.9 +0.3	+1.1 +0.2	+0.1 −0.1	+2.4 −2.4	+2.9 −2.9
	0.26	$1.63 \cdot 10^{-1}$	44	+17 −13	+5.1 −4.9	+1.0 −1.7	+0.5 +0.0	−0.7 +1.8	+1.6 −1.0	+0.1 −0.1	+2.4 −2.4	+2.9 −2.9
1431	0.09	$5.65 \cdot 10^{-1}$	79	+13 −10	+4.8 −4.8	+0.3 −0.7	+1.7 −1.4	+0.6 +0.3	+0.7 −1.3	+0.1 −0.1	+2.4 −2.4	+2.8 −2.8
	0.14	$2.69 \cdot 10^{-1}$	55	+15 −12	+4.6 −4.9	+1.0 −0.5	+0.9 −1.9	−1.1 +0.9	+0.4 +0.0	+0.1 −0.1	+2.4 −2.4	+2.8 −2.8
	0.20	$1.92 \cdot 10^{-1}$	41	+18 −13	+5.0 −5.3	+1.1 −0.7	+2.1 −1.7	−1.3 +0.7	+0.8 −2.0	+0.0 −0.0	+2.4 −2.4	+2.8 −2.8
	0.29	$1.29 \cdot 10^{-1}$	41	+18 −13	+4.8 −4.7	+1.0 −0.9	+0.9 −1.5	−0.6 +1.6	−0.1 −0.1	+0.2 −0.2	+2.4 −2.4	+2.8 −2.8

Table 3. Continued

Q^2 (GeV^2)	x	$\mathrm{d}^2\sigma/\mathrm{d}x\mathrm{d}Q^2$ (pb/GeV^2)	N	δ_s (%)	δ_t (%)	δ_u (%)	δ_1 (%)	δ_2 (%)	δ_3 (%)	δ_4 (%)	δ_5 (%)	δ_6 (%)
1672	0.10	$3.25 \cdot 10^{-1}$	57	$^{+15}_{-11}$	$^{+4.3}_{-4.2}$	$^{+0.3}_{-0.5}$	$^{+1.2}_{-0.7}$	$^{-0.3}_{-0.2}$	$^{+0.4}_{-0.2}$	$^{+0.1}_{-0.1}$	$^{+2.4}_{-2.4}$	$^{+2.5}_{-2.5}$
	0.15	$2.04 \cdot 10^{-1}$	52	$^{+16}_{-12}$	$^{+4.6}_{-4.5}$	$^{+0.4}_{-0.5}$	$^{+1.3}_{-0.5}$	$^{-1.2}_{+1.6}$	$^{+0.3}_{-1.0}$	$^{+0.1}_{-0.1}$	$^{+2.4}_{-2.4}$	$^{+2.5}_{-2.5}$
	0.22	$1.03 \cdot 10^{-1}$	28	$^{+23}_{-15}$	$^{+4.2}_{-4.6}$	$^{+0.1}_{-0.5}$	$^{+0.9}_{-1.6}$	$^{-0.1}_{-0.6}$	$^{+0.3}_{-0.8}$	$^{+0.0}_{-0.0}$	$^{+2.4}_{-2.4}$	$^{+2.5}_{-2.5}$
	0.31	$3.74 \cdot 10^{-2}$	16	$^{+32}_{-20}$	$^{+5.1}_{-5.3}$	$^{+1.2}_{-1.5}$	$^{+1.0}_{-1.9}$	$^{-2.0}_{+2.5}$	$^{+0.1}_{-1.1}$	$^{+0.3}_{-0.3}$	$^{+2.4}_{-2.4}$	$^{+2.5}_{-2.5}$
1951	0.07	$3.91 \cdot 10^{-1}$	60	$^{+15}_{-11}$	$^{+4.1}_{-4.3}$	$^{+0.3}_{-0.7}$	$^{+1.0}_{-0.8}$	$^{-1.1}_{+0.5}$	$^{+0.2}_{-0.9}$	$^{+0.0}_{-0.0}$	$^{+2.4}_{-2.4}$	$^{+2.2}_{-2.2}$
	0.11	$1.86 \cdot 10^{-1}$	39	$^{+19}_{-14}$	$^{+4.9}_{-4.4}$	$^{+0.7}_{-0.6}$	$^{+2.4}_{-1.3}$	$^{+1.2}_{-0.7}$	$^{+0.7}_{-1.0}$	$^{+0.1}_{-0.1}$	$^{+2.4}_{-2.4}$	$^{+2.2}_{-2.2}$
	0.17	$1.22 \cdot 10^{-1}$	37	$^{+19}_{-14}$	$^{+4.1}_{-4.9}$	$^{+0.2}_{-2.7}$	$^{+0.3}_{+0.2}$	$^{-1.2}_{+0.5}$	$^{+0.6}_{+0.7}$	$^{+0.1}_{-0.1}$	$^{+2.4}_{-2.4}$	$^{+2.2}_{-2.2}$
	0.24	$7.22 \cdot 10^{-2}$	26	$^{+24}_{-16}$	$^{+5.0}_{-4.5}$	$^{+0.9}_{-0.8}$	$^{+2.6}_{-0.4}$	$^{-1.9}_{+1.1}$	$^{+0.2}_{-0.6}$	$^{+0.1}_{-0.1}$	$^{+2.4}_{-2.4}$	$^{+2.2}_{-2.2}$
	0.34	$3.48 \cdot 10^{-2}$	18	$^{+30}_{-19}$	$^{+4.8}_{-4.7}$	$^{+1.8}_{-1.8}$	$^{-0.3}_{-0.2}$	$^{-1.1}_{+1.9}$	$^{-0.6}_{-1.0}$	$^{+0.4}_{-0.4}$	$^{+2.4}_{-2.4}$	$^{+2.2}_{-2.2}$
2273	0.07	$3.25 \cdot 10^{-1}$	62	$^{+14}_{-11}$	$^{+4.5}_{-4.7}$	$^{+0.5}_{-1.2}$	$^{+1.6}_{-2.0}$	$^{-0.9}_{+0.2}$	$^{+1.2}_{-0.5}$	$^{+0.0}_{+0.0}$	$^{+2.4}_{-2.4}$	$^{+2.2}_{-2.2}$
	0.12	$1.19 \cdot 10^{-1}$	31	$^{+21}_{-15}$	$^{+4.2}_{-4.8}$	$^{+0.6}_{-1.0}$	$^{+0.7}_{-2.4}$	$^{+0.5}_{-0.6}$	$^{+0.9}_{-0.5}$	$^{+0.1}_{-0.1}$	$^{+2.4}_{-2.4}$	$^{+2.2}_{-2.2}$
	0.18	$7.59 \cdot 10^{-2}$	29	$^{+22}_{-15}$	$^{+4.2}_{-4.5}$	$^{+0.3}_{-0.9}$	$^{+0.6}_{-1.1}$	$^{-1.6}_{+1.3}$	$^{+0.5}_{-0.6}$	$^{+0.1}_{-0.1}$	$^{+2.4}_{-2.4}$	$^{+2.2}_{-2.2}$
	0.26	$5.21 \cdot 10^{-2}$	23	$^{+25}_{-17}$	$^{+4.6}_{-4.5}$	$^{+0.6}_{-0.7}$	$^{+0.7}_{-1.9}$	$^{-0.5}_{+1.1}$	$^{+1.8}_{-0.2}$	$^{+0.1}_{-0.1}$	$^{+2.4}_{-2.4}$	$^{+2.2}_{-2.2}$
	0.37	$1.60 \cdot 10^{-2}$	10	$^{+43}_{-23}$	$^{+6.0}_{-4.4}$	$^{+2.5}_{-0.8}$	$^{+2.0}_{-0.8}$	$^{-1.6}_{+2.5}$	$^{+1.7}_{-0.1}$	$^{+0.5}_{-0.5}$	$^{+2.4}_{-2.4}$	$^{+2.2}_{-2.2}$
2644	0.09	$1.70 \cdot 10^{-1}$	41	$^{+18}_{-13}$	$^{+4.7}_{-4.6}$	$^{+0.6}_{-1.8}$	$^{+2.1}_{-1.3}$	$^{-0.9}_{+0.8}$	$^{+1.0}_{-0.8}$	$^{+0.1}_{-0.1}$	$^{+2.4}_{-2.4}$	$^{+2.1}_{-2.1}$
	0.14	$7.79 \cdot 10^{-2}$	29	$^{+22}_{-15}$	$^{+4.2}_{-4.5}$	$^{+0.2}_{-0.6}$	$^{+1.4}_{-1.7}$	$^{+0.3}_{+0.3}$	$^{+0.7}_{-1.2}$	$^{+0.1}_{-0.1}$	$^{+2.4}_{-2.4}$	$^{+2.1}_{-2.1}$
	0.21	$2.68 \cdot 10^{-2}$	12	$^{+38}_{-21}$	$^{+4.1}_{-4.5}$	$^{+0.4}_{-0.2}$	$^{+0.9}_{-0.4}$	$^{-2.1}_{+0.7}$	$^{+0.0}_{+0.0}$	$^{+0.0}_{-0.0}$	$^{+2.4}_{-2.4}$	$^{+2.1}_{-2.1}$
	0.29	$3.26 \cdot 10^{-2}$	19	$^{+29}_{-18}$	$^{+4.9}_{-4.1}$	$^{+2.0}_{-0.3}$	$^{+1.0}_{-0.9}$	$^{+0.3}_{+2.0}$	$^{-0.5}_{-0.8}$	$^{+0.2}_{-0.2}$	$^{+2.4}_{-2.4}$	$^{+2.1}_{-2.1}$
	0.40	$1.47 \cdot 10^{-2}$	11	$^{+40}_{-22}$	$^{+4.7}_{-6.3}$	$^{+1.1}_{-2.1}$	$^{+0.9}_{-1.7}$	$^{-3.9}_{+2.2}$	$^{+0.2}_{-1.2}$	$^{+0.5}_{-0.5}$	$^{+2.4}_{-2.4}$	$^{+2.1}_{-2.1}$
3073	0.06	$1.16 \cdot 10^{-1}$	20	$^{+28}_{-18}$	$^{+4.9}_{-4.7}$	$^{+0.4}_{-1.3}$	$^{+2.3}_{-2.3}$	$^{+1.3}_{-0.3}$	$^{+1.5}_{-0.7}$	$^{+0.1}_{-0.1}$	$^{+2.4}_{-2.4}$	$^{+2.0}_{-2.0}$
	0.10	$9.39 \cdot 10^{-2}$	25	$^{+24}_{-16}$	$^{+4.1}_{-5.8}$	$^{+0.9}_{-3.8}$	$^{+0.8}_{-1.5}$	$^{-1.5}_{+0.7}$	$^{+0.1}_{-0.4}$	$^{+0.0}_{-0.0}$	$^{+2.4}_{-2.4}$	$^{+2.0}_{-2.0}$
	0.15	$4.29 \cdot 10^{-2}$	19	$^{+29}_{-18}$	$^{+4.6}_{-4.2}$	$^{+0.6}_{-0.4}$	$^{+2.0}_{-1.6}$	$^{+0.4}_{+0.1}$	$^{+1.2}_{-0.4}$	$^{+0.1}_{-0.1}$	$^{+2.4}_{-2.4}$	$^{+2.0}_{-2.0}$
	0.23	$2.53 \cdot 10^{-2}$	14	$^{+35}_{-20}$	$^{+7.7}_{-4.9}$	$^{+6.5}_{-0.3}$	$^{+0.6}_{-1.6}$	$^{-2.5}_{+1.6}$	$^{+0.3}_{-0.8}$	$^{+0.0}_{-0.0}$	$^{+2.4}_{-2.4}$	$^{+2.0}_{-2.0}$
	0.32	$1.46 \cdot 10^{-2}$	11	$^{+40}_{-22}$	$^{+4.0}_{-4.1}$	$^{+0.4}_{-0.6}$	$^{+0.0}_{-0.4}$	$^{-1.3}_{+0.1}$	$^{+0.3}_{+0.9}$	$^{+0.2}_{-0.2}$	$^{+2.4}_{-2.4}$	$^{+2.0}_{-2.0}$
	0.43	$9.60 \cdot 10^{-4}$	1	$^{+220}_{-30}$	$^{+6.8}_{-4.5}$	$^{+1.4}_{-1.7}$	$^{-0.8}_{+0.0}$	$^{-1.2}_{+5.4}$	$^{+0.4}_{-0.4}$	$^{+0.5}_{-0.5}$	$^{+2.4}_{-2.4}$	$^{+2.0}_{-2.0}$
3568	0.07	$1.22 \cdot 10^{-1}$	28	$^{+23}_{-15}$	$^{+4.0}_{-4.6}$	$^{+0.9}_{-1.2}$	$^{+1.1}_{-2.3}$	$^{-0.0}_{-0.2}$	$^{+0.7}_{-0.7}$	$^{+0.0}_{-0.0}$	$^{+2.4}_{-2.4}$	$^{+1.7}_{-1.7}$
	0.11	$3.80 \cdot 10^{-2}$	14	$^{+35}_{-20}$	$^{+4.1}_{-8.2}$	$^{+0.4}_{-7.1}$	$^{+0.9}_{-1.4}$	$^{+0.2}_{+1.3}$	$^{+0.5}_{-0.8}$	$^{+0.1}_{-0.1}$	$^{+2.4}_{-2.4}$	$^{+1.7}_{-1.7}$
	0.17	$3.06 \cdot 10^{-2}$	16	$^{+32}_{-19}$	$^{+4.1}_{-4.4}$	$^{+0.2}_{-0.7}$	$^{+1.7}_{-1.8}$	$^{-0.9}_{-0.1}$	$^{+0.7}_{-1.2}$	$^{+0.1}_{-0.1}$	$^{+2.4}_{-2.4}$	$^{+1.7}_{-1.7}$
	0.25	$2.37 \cdot 10^{-2}$	17	$^{+31}_{-19}$	$^{+4.7}_{-4.2}$	$^{+0.2}_{-0.4}$	$^{+1.5}_{-1.3}$	$^{-1.4}_{+2.3}$	$^{+1.1}_{-0.5}$	$^{+0.0}_{-0.0}$	$^{+2.4}_{-2.4}$	$^{+1.7}_{-1.7}$
	0.35	$1.02 \cdot 10^{-2}$	10	$^{+43}_{-23}$	$^{+4.6}_{-4.6}$	$^{+1.9}_{-0.9}$	$^{+0.8}_{-2.0}$	$^{-0.9}_{+1.7}$	$^{+0.8}_{-1.4}$	$^{+0.3}_{-0.3}$	$^{+2.4}_{-2.4}$	$^{+1.7}_{-1.7}$
	0.47	$8.33 \cdot 10^{-4}$	1	$^{+220}_{-30}$	$^{+7.5}_{-5.7}$	$^{+2.9}_{-1.9}$	$^{+3.7}_{-2.5}$	$^{-2.8}_{+4.3}$	$^{+1.2}_{+0.1}$	$^{+0.6}_{-0.6}$	$^{+2.4}_{-2.4}$	$^{+1.7}_{-1.7}$
4145	0.08	$5.23 \cdot 10^{-2}$	15	$^{+33}_{-20}$	$^{+7.8}_{-4.0}$	$^{+6.5}_{-1.2}$	$^{+2.0}_{-0.6}$	$^{+1.3}_{-0.2}$	$^{+0.6}_{-0.9}$	$^{+0.0}_{-0.0}$	$^{+2.4}_{-2.4}$	$^{+1.6}_{-1.6}$
	0.13	$3.39 \cdot 10^{-2}$	16	$^{+32}_{-19}$	$^{+4.1}_{-4.2}$	$^{+0.3}_{-0.8}$	$^{+1.3}_{-0.3}$	$^{-1.8}_{+1.1}$	$^{+0.3}_{-0.6}$	$^{+0.1}_{-0.1}$	$^{+2.4}_{-2.4}$	$^{+1.6}_{-1.6}$
	0.19	$1.88 \cdot 10^{-2}$	13	$^{+36}_{-21}$	$^{+4.0}_{-4.2}$	$^{+0.8}_{-0.5}$	$^{+1.3}_{-1.6}$	$^{-0.7}_{+0.4}$	$^{+0.2}_{-0.9}$	$^{+0.1}_{-0.1}$	$^{+2.4}_{-2.4}$	$^{+1.6}_{-1.6}$
	0.28	$1.49 \cdot 10^{-2}$	14	$^{+35}_{-20}$	$^{+4.0}_{-4.2}$	$^{+0.3}_{-0.6}$	$^{+0.4}_{-1.1}$	$^{-1.3}_{+1.4}$	$^{+0.2}_{-1.0}$	$^{+0.1}_{-0.1}$	$^{+2.4}_{-2.4}$	$^{+1.6}_{-1.6}$
	0.39	$3.33 \cdot 10^{-3}$	4	$^{+79}_{-29}$	$^{+5.6}_{-3.8}$	$^{+2.5}_{-0.3}$	$^{+1.8}_{+0.0}$	$^{-0.7}_{+2.5}$	$^{+0.6}_{+1.3}$	$^{+0.4}_{-0.4}$	$^{+2.4}_{-2.4}$	$^{+1.6}_{-1.6}$
	0.51	$1.36 \cdot 10^{-3}$	2	$^{+130}_{-32}$	$^{+5.9}_{-8.9}$	$^{+3.3}_{-2.6}$	$^{+1.5}_{-0.6}$	$^{-6.2}_{+2.9}$	$^{-4.1}_{-1.7}$	$^{+0.7}_{-0.7}$	$^{+2.4}_{-2.4}$	$^{+1.6}_{-1.6}$
4806	0.11	$3.28 \cdot 10^{-2}$	14	$^{+35}_{-20}$	$^{+4.5}_{-4.4}$	$^{+0.2}_{-0.7}$	$^{+1.5}_{-2.4}$	$^{+1.1}_{+1.1}$	$^{+1.8}_{-0.4}$	$^{+0.0}_{+0.0}$	$^{+2.4}_{-2.4}$	$^{+1.4}_{-1.4}$
	0.16	$1.70 \cdot 10^{-2}$	10	$^{+43}_{-23}$	$^{+4.5}_{-4.5}$	$^{+0.3}_{-0.8}$	$^{+0.6}_{-1.2}$	$^{-2.2}_{+2.6}$	$^{+0.9}_{-0.9}$	$^{+0.1}_{-0.1}$	$^{+2.4}_{-2.4}$	$^{+1.4}_{-1.4}$
	0.23	$1.38 \cdot 10^{-2}$	13	$^{+36}_{-21}$	$^{+4.1}_{-4.1}$	$^{+0.6}_{-0.3}$	$^{+1.7}_{+0.5}$	$^{-1.6}_{-0.6}$	$^{+0.6}_{-0.9}$	$^{+0.0}_{-0.0}$	$^{+2.4}_{-2.4}$	$^{+1.4}_{-1.4}$
	0.33	$5.78 \cdot 10^{-3}$	7	$^{+54}_{-25}$	$^{+4.1}_{-5.2}$	$^{+1.1}_{-0.3}$	$^{+1.3}_{-2.2}$	$^{-2.4}_{+1.0}$	$^{+0.4}_{-1.8}$	$^{+0.2}_{-0.2}$	$^{+2.4}_{-2.4}$	$^{+1.4}_{-1.4}$
	0.44	$5.73 \cdot 10^{-3}$	8	$^{+49}_{-24}$	$^{+5.0}_{-5.4}$	$^{+1.2}_{-2.8}$	$^{+0.7}_{-0.7}$	$^{-2.6}_{+3.2}$	$^{+0.2}_{-1.2}$	$^{+0.4}_{-0.4}$	$^{+2.4}_{-2.4}$	$^{+1.4}_{-1.4}$
	0.56	$1.23 \cdot 10^{-3}$	2	$^{+130}_{-32}$	$^{+7.8}_{-12}$	$^{+4.3}_{-1.1}$	$^{-3.2}_{-3.9}$	$^{-9.8}_{+3.3}$	$^{+4.3}_{+0.1}$	$^{+0.4}_{-0.4}$	$^{+2.4}_{-2.4}$	$^{+1.4}_{-1.4}$

Table 3. Continued

Q^2 (GeV^2)	x	$\mathrm{d}^2\sigma/\mathrm{d}x\mathrm{d}Q^2$ (pb/GeV^2)	N	δ_s (%)	δ_t (%)	δ_u (%)	δ_1 (%)	δ_2 (%)	δ_3 (%)	δ_4 (%)	δ_5 (%)	δ_6 (%)
5561	0.12	$1.90 \cdot 10^{-2}$	10	+43 −24	+4.1 −4.5	+0.2 −1.3	+1.8 −1.2	−1.7 −0.5	+1.2 −1.4	+0.0 −0.0	+2.4 −2.4	+1.2 −1.2
	0.18	$1.03 \cdot 10^{-2}$	8	+49 −24	+5.8 −3.7	+0.3 −0.4	+0.8 −1.1	+1.0 +4.5	+0.1 −0.1	+0.1 −0.1	+2.4 −2.4	+1.2 −1.2
	0.26	$4.73 \cdot 10^{-3}$	6	+60 −26	+4.0 −4.0	+0.5 −0.3	+1.2 −1.2	−1.5 +1.5	+0.0 −0.4	+0.1 −0.1	+2.4 −2.4	+1.2 −1.2
	0.37	$6.69 \cdot 10^{-4}$	1	+220 −30	+4.2 −4.3	+1.2 −0.6	+0.8 −0.4	−2.4 +1.3	+0.6 +0.8	+0.3 −0.3	+2.4 −2.4	+1.2 −1.2
	0.49	$1.70 \cdot 10^{-3}$	3	+96 −30	+5.6 −7.2	+1.7 −3.5	−2.1 −4.0	−2.4 +3.9	+0.9 −0.5	+0.6 −0.6	+2.4 −2.4	+1.2 −1.2
	0.61	$< 6.44 \cdot 10^{-4}$	0									
6966	0.14	$1.37 \cdot 10^{-2}$	22	+26 −17	+4.1 −5.2	+0.9 −3.1	+1.8 −2.1	−0.9 +0.1	+0.8 −0.7	+0.0 −0.0	+2.4 −2.4	+1.0 −1.0
	0.21	$6.68 \cdot 10^{-3}$	14	+35 −20	+4.1 −4.2	+0.4 −0.8	+1.5 −1.5	−1.8 +1.3	+0.7 −0.5	+0.0 −0.0	+2.4 −2.4	+1.0 −1.0
	0.30	$2.06 \cdot 10^{-3}$	7	+54 −25	+4.6 −4.1	+0.3 −0.5	+1.8 −0.9	−2.0 +2.3	+0.7 −0.6	+0.2 −0.2	+2.4 −2.4	+1.0 −1.0
	0.41	$1.87 \cdot 10^{-3}$	7	+54 −25	+4.7 −4.4	+0.8 −0.3	+1.7 −0.8	−2.4 +2.5	+0.6 −0.8	+0.4 −0.4	+2.4 −2.4	+1.0 −1.0
	0.53	$2.14 \cdot 10^{-4}$	1	+220 −30	+6.1 −4.9	+0.3 −0.7	+1.6 −0.8	−3.2 +4.7	+0.6 −1.0	+0.5 −0.5	+2.4 −2.4	+1.0 −1.0
	0.69	$1.17 \cdot 10^{-4}$	1	+220 −30	+18 −17	+14 −15	+4.2 +4.5	−7.0 +9.5	−0.5 −1.4	+0.6 −0.6	+2.4 −2.4	+1.0 −1.0
9059	0.13	$5.13 \cdot 10^{-3}$	4	+79 −29	+8.1 −23	+0.9 −22	+2.8 −3.4	+6.6 −2.8	+1.7 −1.5	+0.0 −0.0	+2.4 −2.4	+0.7 −0.7
	0.19	$3.64 \cdot 10^{-3}$	8	+49 −24	+4.4 −5.0	+0.7 −2.1	+2.3 −2.5	−1.0 +1.1	+1.1 −1.5	+0.1 −0.1	+2.4 −2.4	+0.7 −0.7
	0.27	$3.10 \cdot 10^{-3}$	11	+40 −22	+4.0 −4.3	+0.5 −1.0	+1.1 −1.6	−1.8 +1.8	+0.6 −0.7	+0.1 −0.1	+2.4 −2.4	+0.7 −0.7
	0.38	$3.84 \cdot 10^{-4}$	2	+130 −32	+4.5 −5.7	+0.8 −0.6	+0.8 +0.3	−4.5 +2.7	+0.5 −0.3	+0.4 −0.4	+2.4 −2.4	+0.7 −0.7
	0.51	$1.73 \cdot 10^{-4}$	1	+220 −30	+5.5 −4.9	+1.5 −1.2	+1.2 −1.0	−3.1 +3.8	+0.6 −0.7	+0.6 −0.6	+2.4 −2.4	+0.7 −0.7
	0.64	$< 1.83 \cdot 10^{-4}$	0									
	0.78	$9.12 \cdot 10^{-5}$	1	+220 −30	+9.9 −13	+1.8 −1.1	+1.0 −1.6	−12 +8.8	+0.4 −0.3	+2.2 −2.2	+2.4 −2.4	+0.7 −0.7
	0.93	$< 1.08 \cdot 10^{-5}$	0									
15 072	0.61	$8.57 \cdot 10^{-5}$	3	+96 −30	+22 −25	+18 −20	−5.9 −9.5	−8.9 +11	+0.4 −1.1	+0.9 −0.9	+2.4 −2.4	+0.5 −0.5
	0.75	$< 1.97 \cdot 10^{-5}$	0									
	0.91	$< 2.04 \cdot 10^{-6}$	0									

Table 4. The integral cross section table for 98–99 e^-p NC scattering. The first two columns of the table contain the Q^2 and x_{edge} values for the bin, the third contains the measured cross section $\int_{x_{\mathrm{edge}}}^{1} \mathrm{d}^2\sigma/\mathrm{d}x\mathrm{d}Q^2$ corrected to the electroweak Born level or the upper limit in case of zero observed events, the fourth contains the number of events reconstructed in the bin, N, the fifth contains the statistical uncertainty, δ_s, and the sixth contains the total systematic uncertainty, δ_t. The right part of the table lists the total uncorrelated systematic uncertainty, δ_u, followed by the bin-to-bin correlated systematic uncertainties δ_1–δ_6 defined in the text. The upper (lower) numbers refer to the variation of the cross section, whereas the signs of the numbers reflect the direction of change in the cross sections. Note that the normalization uncertainty, δ_7, is not listed

Q^2 (GeV^2)	x_{edge}	$\int_{x_{\mathrm{edge}}}^{1} \mathrm{d}^2\sigma/\mathrm{d}x\mathrm{d}Q^2$ (pb/GeV^2)	N	δ_s (%)	δ_t (%)	δ_u (%)	δ_1 (%)	δ_2 (%)	δ_3 (%)	δ_4 (%)	δ_5 (%)	δ_6 (%)
648	0.22	$8.74 \cdot 10^{-2}$	14	+35 −20	+8.7 −8.2	+3.7 −1.9	−5.9 +5.6	+0.0 +0.0	−3.0 +3.4	+0.3 −0.3	+1.6 −1.6	+3.4 −3.4
761	0.24	$7.12 \cdot 10^{-2}$	54	+16 −12	+5.5 −6.0	+0.5 −0.5	−3.7 +2.7	+0.0 −0.1	−1.9 +2.1	+0.2 −0.2	+1.6 −1.6	+3.3 −3.3
891	0.26	$3.44 \cdot 10^{-2}$	56	+15 −12	+4.5 −4.4	+1.3 −0.6	+0.3 −0.6	+0.0 −0.1	+0.6 −0.6	+0.2 −0.2	+1.6 −1.6	+3.2 −3.2
1045	0.29	$2.29 \cdot 10^{-2}$	54	+16 −12	+4.5 −4.5	+1.3 −0.9	+1.5 −1.5	+0.0 −0.2	+0.7 −1.0	+0.3 −0.3	+1.6 −1.6	+2.9 −2.9
1224	0.31	$9.38 \cdot 10^{-3}$	28	+23 −15	+4.9 −5.5	+0.2 −0.5	+2.4 −3.6	−0.2 −0.2	+1.4 −1.1	+0.2 −0.2	+1.6 −1.6	+2.9 −2.9
1431	0.34	$8.51 \cdot 10^{-3}$	29	+22 −15	+5.4 −5.5	+0.2 −0.1	+3.6 −2.9	+0.3 +0.2	+0.6 −2.4	+0.2 −0.2	+1.6 −1.6	+2.8 −2.8
1672	0.36	$6.31 \cdot 10^{-3}$	25	+24 −16	+4.4 −4.5	+0.8 −0.3	+1.4 −1.9	−0.4 −0.5	+1.7 −1.6	+0.2 −0.2	+1.6 −1.6	+2.5 −2.5
1951	0.39	$3.34 \cdot 10^{-3}$	16	+32 −19	+6.9 −4.3	+1.8 −1.6	+5.1 −1.6	+1.1 +1.0	+2.0 −0.9	+0.2 −0.2	+1.6 −1.6	+2.2 −2.2
2273	0.43	$1.61 \cdot 10^{-3}$	8	+49 −24	+5.6 −7.5	+3.1 −2.0	+2.9 −5.4	−0.5 −0.5	+1.0 −3.1	+0.2 −0.2	+1.6 −1.6	+2.2 −2.2
2644	0.46	$8.11 \cdot 10^{-4}$	5	+67 −27	+6.3 −5.6	+2.1 −0.2	+3.9 −4.0	+1.4 +1.4	+1.9 −1.8	+0.2 −0.2	+1.6 −1.6	+2.1 −2.1

Table 4. Continued

Q^2 (GeV^2)	x_{edge}	$\int_{x_{\text{edge}}}^{1} \mathrm{d}^2\sigma/\mathrm{d}x\mathrm{d}Q^2$ (pb/GeV^2)	N	δ_s (%)	δ_t (%)	δ_u (%)	δ_1 (%)	δ_2 (%)	δ_3 (%)	δ_4 (%)	δ_5 (%)	δ_6 (%)
3073	0.50	$< 1.62\cdot 10^{-4}$	0									
3568	0.54	$2.43\cdot 10^{-4}$	2	$^{+130}_{-32}$	$^{+7.6}_{-4.5}$	$^{+3.3}_{-0.5}$	$^{+5.3}_{-2.5}$	$^{+1.1}_{+0.8}$	$^{+2.5}_{-1.9}$	$^{+0.2}_{-0.2}$	$^{+1.6}_{-1.6}$	$^{+1.7}_{-1.7}$
4145	0.58	$2.06\cdot 10^{-4}$	2	$^{+130}_{-32}$	$^{+6.2}_{-4.6}$	$^{+0.7}_{-0.7}$	$^{+3.6}_{-1.7}$	$^{+0.1}_{+0.1}$	$^{+3.9}_{-2.8}$	$^{+0.1}_{-0.1}$	$^{+1.6}_{-1.6}$	$^{+1.6}_{-1.6}$
4806	0.63	$< 1.02\cdot 10^{-4}$	0									
5561	0.68	$< 8.95\cdot 10^{-5}$	0									
6966	0.79	$< 1.38\cdot 10^{-5}$	0									

Table 5. The cross section table for 99–00 e^+p NC scattering. The first two columns of the table contain the Q^2 and x values at which the cross section is quoted, the third contains the measured cross section $\mathrm{d}^2\sigma/\mathrm{d}x\mathrm{d}Q^2$ corrected to the electroweak Born level or the upper limit in case of zero observed events, the fourth contains the number of events reconstructed in the bin, N, the fifth contains the statistical uncertainty, δ_s, and the sixth contains the total systematic uncertainty, δ_t. The right part of the table lists the total uncorrelated systematic uncertainty, δ_u, followed by the bin-to-bin correlated systematic uncertainties δ_1–δ_6 defined in the text. The upper (lower) numbers refer to the variation of the cross section, whereas the signs of the numbers reflect the direction of change in the cross sections. Note that the normalization uncertainty, δ_7, is not listed

Q^2 (GeV^2)	x	$\mathrm{d}^2\sigma/\mathrm{d}x\mathrm{d}Q^2$ (pb/GeV^2)	N	δ_s (%)	δ_t (%)	δ_u (%)	δ_1 (%)	δ_2 (%)	δ_3 (%)	δ_4 (%)	δ_5 (%)	δ_6 (%)
648	0.08	3.02	255	$^{+6.6}_{-5.9}$	$^{+7.1}_{-6.3}$	$^{+1.3}_{-1.0}$	$^{+5.8}_{-5.2}$	$^{-0.9}_{+1.8}$	$^{+0.2}_{-0.3}$	$^{+0.3}_{-0.3}$	$^{+2.4}_{-2.4}$	$^{+0.7}_{-0.7}$
	0.13	1.86	116	$^{+10}_{-8.4}$	$^{+6.9}_{-6.8}$	$^{+2.1}_{-1.3}$	$^{+5.2}_{-5.6}$	$^{-1.0}_{+0.6}$	$^{+1.8}_{+0.3}$	$^{+0.2}_{-0.2}$	$^{+2.4}_{-2.4}$	$^{+1.2}_{-1.2}$
	0.19	1.05	87	$^{+12}_{-9.6}$	$^{+11}_{-9.4}$	$^{+4.7}_{-3.4}$	$^{+8.6}_{-7.4}$	$^{-1.2}_{+1.8}$	$^{+1.0}_{-2.3}$	$^{+0.1}_{-0.1}$	$^{+2.4}_{-2.4}$	$^{+1.9}_{-1.9}$
761	0.09	1.85	403	$^{+5.2}_{-4.7}$	$^{+4.1}_{-4.4}$	$^{+0.4}_{-0.9}$	$^{+2.1}_{-2.6}$	$^{-0.6}_{+0.7}$	$^{+0.0}_{+0.1}$	$^{+0.2}_{-0.2}$	$^{+2.4}_{-2.4}$	$^{+0.8}_{-0.8}$
	0.14	$9.89\cdot 10^{-1}$	216	$^{+7.3}_{-6.3}$	$^{+5.3}_{-4.3}$	$^{+0.6}_{-1.2}$	$^{+3.6}_{-2.0}$	$^{-0.7}_{+0.9}$	$^{+0.9}_{-0.2}$	$^{+0.0}_{-0.0}$	$^{+2.4}_{-2.4}$	$^{+1.3}_{-1.3}$
	0.21	$6.18\cdot 10^{-1}$	161	$^{+8.5}_{-7.3}$	$^{+5.2}_{-5.7}$	$^{+1.0}_{-0.7}$	$^{+1.9}_{-3.1}$	$^{-1.4}_{+1.8}$	$^{+2.0}_{-2.4}$	$^{+0.2}_{-0.2}$	$^{+2.4}_{-2.4}$	$^{+2.2}_{-2.2}$
891	0.10	1.23	471	$^{+4.8}_{-4.4}$	$^{+3.5}_{-3.8}$	$^{+0.3}_{-1.1}$	$^{+0.5}_{-1.0}$	$^{-0.7}_{+0.2}$	$^{+0.3}_{-0.2}$	$^{+0.1}_{-0.1}$	$^{+2.4}_{-2.4}$	$^{+0.9}_{-0.9}$
	0.15	$7.65\cdot 10^{-1}$	301	$^{+6.1}_{-5.4}$	$^{+4.1}_{-3.9}$	$^{+1.6}_{-0.4}$	$^{-0.6}_{+0.1}$	$^{-0.7}_{+1.1}$	$^{+0.7}_{-1.1}$	$^{+0.1}_{-0.1}$	$^{+2.4}_{-2.4}$	$^{+1.5}_{-1.5}$
	0.22	$3.64\cdot 10^{-1}$	189	$^{+7.9}_{-6.8}$	$^{+5.3}_{-4.7}$	$^{+2.2}_{-0.3}$	$^{+2.4}_{-1.5}$	$^{-1.7}_{+1.1}$	$^{+0.9}_{-1.1}$	$^{+0.2}_{-0.2}$	$^{+2.4}_{-2.4}$	$^{+2.3}_{-2.3}$
1045	0.07	1.49	532	$^{+4.5}_{-4.2}$	$^{+4.5}_{-4.2}$	$^{+0.7}_{-0.6}$	$^{-2.3}_{+2.9}$	$^{-0.1}_{+0.2}$	$^{-0.6}_{+0.6}$	$^{+0.1}_{-0.1}$	$^{+2.4}_{-2.4}$	$^{+0.6}_{-0.6}$
	0.11	$7.98\cdot 10^{-1}$	388	$^{+5.3}_{-4.8}$	$^{+3.8}_{-3.7}$	$^{+0.9}_{-0.1}$	$^{-0.2}_{+0.8}$	$^{-1.4}_{+1.0}$	$^{+0.0}_{-0.3}$	$^{+0.1}_{-0.1}$	$^{+2.4}_{-2.4}$	$^{+1.0}_{-1.0}$
	0.17	$4.82\cdot 10^{-1}$	253	$^{+6.7}_{-5.9}$	$^{+4.1}_{-3.9}$	$^{+0.9}_{-0.7}$	$^{+0.1}_{+0.5}$	$^{-0.1}_{+0.1}$	$^{+1.3}_{-1.1}$	$^{+0.1}_{-0.1}$	$^{+2.4}_{-2.4}$	$^{+1.7}_{-1.7}$
	0.24	$2.21\cdot 10^{-1}$	173	$^{+8.2}_{-7.1}$	$^{+4.9}_{-5.1}$	$^{+0.6}_{-1.1}$	$^{-2.0}_{+1.9}$	$^{-0.8}_{+1.1}$	$^{+1.3}_{-1.6}$	$^{+0.2}_{-0.2}$	$^{+2.4}_{-2.4}$	$^{+2.5}_{-2.5}$
1224	0.07	1.03	444	$^{+5.0}_{-4.5}$	$^{+3.7}_{-3.8}$	$^{+0.8}_{-0.2}$	$^{-1.7}_{+1.4}$	$^{-0.1}_{+0.1}$	$^{-0.4}_{+0.4}$	$^{+0.2}_{-0.2}$	$^{+2.4}_{-2.4}$	$^{+0.6}_{-0.6}$
	0.12	$4.81\cdot 10^{-1}$	294	$^{+6.2}_{-5.5}$	$^{+3.9}_{-4.0}$	$^{+0.4}_{-0.9}$	$^{-1.7}_{+1.6}$	$^{-0.7}_{+0.1}$	$^{-0.1}_{-0.3}$	$^{+0.0}_{-0.0}$	$^{+2.4}_{-2.4}$	$^{+1.1}_{-1.1}$
	0.18	$2.99\cdot 10^{-1}$	208	$^{+7.4}_{-6.4}$	$^{+4.0}_{-4.2}$	$^{+0.5}_{-0.5}$	$^{-0.8}_{+0.7}$	$^{-1.0}_{+0.1}$	$^{+0.9}_{-1.4}$	$^{+0.1}_{-0.1}$	$^{+2.4}_{-2.4}$	$^{+1.8}_{-1.8}$
	0.26	$1.31\cdot 10^{-1}$	139	$^{+9.2}_{-7.8}$	$^{+5.9}_{-4.6}$	$^{+0.4}_{-0.6}$	$^{-0.9}_{+0.9}$	$^{-0.2}_{+1.9}$	$^{+3.4}_{-1.2}$	$^{+0.1}_{-0.1}$	$^{+2.4}_{-2.4}$	$^{+2.8}_{-2.8}$
1431	0.09	$5.29\cdot 10^{-1}$	278	$^{+6.4}_{-5.6}$	$^{+3.8}_{-3.5}$	$^{+0.5}_{-0.3}$	$^{-0.4}_{+1.7}$	$^{-0.0}_{-0.4}$	$^{-0.2}_{+0.2}$	$^{+0.1}_{-0.1}$	$^{+2.4}_{-2.4}$	$^{+0.8}_{-0.8}$
	0.14	$2.74\cdot 10^{-1}$	212	$^{+7.3}_{-6.4}$	$^{+4.0}_{-3.8}$	$^{+0.6}_{-0.3}$	$^{-0.8}_{+0.9}$	$^{-0.9}_{+1.4}$	$^{-0.0}_{-0.1}$	$^{+0.0}_{-0.0}$	$^{+2.4}_{-2.4}$	$^{+1.3}_{-1.3}$
	0.20	$1.51\cdot 10^{-1}$	126	$^{+9.7}_{-8.1}$	$^{+4.2}_{-4.7}$	$^{+0.8}_{-1.2}$	$^{-1.4}_{+0.9}$	$^{-0.6}_{+0.4}$	$^{+1.0}_{-1.7}$	$^{+0.2}_{-0.2}$	$^{+2.4}_{-2.4}$	$^{+2.0}_{-2.0}$
	0.29	$0.99\cdot 10^{-1}$	119	$^{+10}_{-8.3}$	$^{+6.0}_{-5.4}$	$^{+1.9}_{-0.1}$	$^{-0.2}_{+2.2}$	$^{-1.8}_{+1.5}$	$^{+2.2}_{-2.1}$	$^{+0.0}_{-0.0}$	$^{+2.4}_{-2.4}$	$^{+3.2}_{-3.2}$
1672	0.10	$3.71\cdot 10^{-1}$	249	$^{+6.8}_{-6.0}$	$^{+3.8}_{-3.9}$	$^{+0.6}_{-0.6}$	$^{-1.6}_{+1.5}$	$^{-0.1}_{+0.3}$	$^{-0.2}_{+0.2}$	$^{+0.1}_{-0.1}$	$^{+2.4}_{-2.4}$	$^{+0.9}_{-0.9}$
	0.15	$1.93\cdot 10^{-1}$	183	$^{+8.0}_{-6.9}$	$^{+3.9}_{-3.9}$	$^{+0.5}_{-0.7}$	$^{-1.1}_{+1.1}$	$^{-0.7}_{+0.7}$	$^{+0.2}_{-0.1}$	$^{+0.1}_{-0.1}$	$^{+2.4}_{-2.4}$	$^{+1.5}_{-1.5}$
	0.22	$1.05\cdot 10^{-1}$	113	$^{+10}_{-8.6}$	$^{+4.2}_{-4.5}$	$^{+0.2}_{-0.8}$	$^{-1.3}_{+0.8}$	$^{-0.3}_{+0.1}$	$^{+1.0}_{-1.4}$	$^{+0.1}_{-0.1}$	$^{+2.4}_{-2.4}$	$^{+2.3}_{-2.3}$
	0.31	$6.10\cdot 10^{-2}$	96	$^{+11}_{-9.2}$	$^{+6.0}_{-5.3}$	$^{+1.0}_{-0.3}$	$^{-0.6}_{+0.6}$	$^{-2.1}_{+2.9}$	$^{+1.7}_{-0.7}$	$^{+0.1}_{-0.1}$	$^{+2.4}_{-2.4}$	$^{+3.4}_{-3.4}$
1951	0.07	$3.77\cdot 10^{-1}$	215	$^{+7.3}_{-6.3}$	$^{+3.6}_{-3.7}$	$^{+0.6}_{-0.4}$	$^{-1.5}_{+1.1}$	$^{-0.0}_{+0.6}$	$^{+0.1}_{-0.1}$	$^{+0.1}_{-0.1}$	$^{+2.4}_{-2.4}$	$^{+0.6}_{-0.6}$
	0.11	$1.89\cdot 10^{-1}$	149	$^{+8.9}_{-7.5}$	$^{+4.1}_{-4.0}$	$^{+0.6}_{-0.9}$	$^{-1.8}_{+2.0}$	$^{-0.3}_{-0.6}$	$^{-0.3}_{+0.2}$	$^{+0.1}_{-0.1}$	$^{+2.4}_{-2.4}$	$^{+1.0}_{-1.0}$
	0.17	$1.10\cdot 10^{-1}$	126	$^{+9.7}_{-8.1}$	$^{+4.3}_{-4.0}$	$^{+1.2}_{-0.4}$	$^{-1.0}_{+1.0}$	$^{-1.2}_{+1.6}$	$^{+0.5}_{-0.4}$	$^{+0.1}_{-0.1}$	$^{+2.4}_{-2.4}$	$^{+1.7}_{-1.7}$
	0.24	$7.26\cdot 10^{-2}$	102	$^{+11}_{-9.0}$	$^{+4.8}_{-4.4}$	$^{+1.1}_{-0.3}$	$^{-0.8}_{+1.9}$	$^{-0.5}_{+0.2}$	$^{+0.9}_{-0.9}$	$^{+0.1}_{-0.1}$	$^{+2.4}_{-2.4}$	$^{+2.5}_{-2.5}$
	0.34	$3.34\cdot 10^{-2}$	69	$^{+14}_{-11}$	$^{+6.0}_{-5.6}$	$^{+0.2}_{-1.0}$	$^{-1.2}_{+0.8}$	$^{-1.7}_{+2.6}$	$^{+1.7}_{-0.9}$	$^{+0.2}_{-0.2}$	$^{+2.4}_{-2.4}$	$^{+3.9}_{-3.9}$

Table 5. Continued

Q^2 (GeV^2)	x	$\mathrm{d}^2\sigma/\mathrm{d}x\mathrm{d}Q^2$ (pb/GeV^2)	N	δ_s (%)	δ_t (%)	δ_u (%)	δ_1 (%)	δ_2 (%)	δ_3 (%)	δ_4 (%)	δ_5 (%)	δ_6 (%)
2273	0.07	$2.41\cdot10^{-1}$	179	$^{+8.1}_{-7.0}$	$^{+4.0}_{-3.8}$	$^{+0.9}_{-0.4}$	$^{-1.4}_{+1.7}$	$^{-1.0}_{+0.8}$	$^{-0.0}_{-0.0}$	$^{+0.2}_{-0.2}$	$^{+2.4}_{-2.4}$	$^{+0.6}_{-0.6}$
	0.12	$1.55\cdot10^{-1}$	150	$^{+8.8}_{-7.5}$	$^{+4.1}_{-4.0}$	$^{+0.6}_{-1.0}$	$^{-1.7}_{+2.0}$	$^{-0.4}_{-0.2}$	$^{-0.5}_{+0.4}$	$^{+0.0}_{-0.0}$	$^{+2.4}_{-2.4}$	$^{+1.1}_{-1.1}$
	0.18	$8.25\cdot10^{-2}$	114	$^{+10}_{-8.5}$	$^{+4.3}_{-4.1}$	$^{+0.2}_{-0.6}$	$^{-0.6}_{+1.3}$	$^{-1.4}_{+1.5}$	$^{+0.2}_{-0.3}$	$^{+0.1}_{-0.1}$	$^{+2.4}_{-2.4}$	$^{+1.8}_{-1.8}$
	0.26	$3.77\cdot10^{-2}$	68	$^{+14}_{-11}$	$^{+5.0}_{-4.5}$	$^{+1.0}_{-0.2}$	$^{-0.7}_{+1.8}$	$^{+0.7}_{+0.4}$	$^{+1.0}_{-1.1}$	$^{+0.1}_{-0.1}$	$^{+2.4}_{-2.4}$	$^{+2.8}_{-2.8}$
	0.37	$1.71\cdot10^{-2}$	40	$^{+18}_{-13}$	$^{+6.6}_{-6.4}$	$^{+0.8}_{-0.3}$	$^{-1.4}_{+2.3}$	$^{-2.8}_{+2.2}$	$^{+1.9}_{-1.4}$	$^{+0.3}_{-0.3}$	$^{+2.4}_{-2.4}$	$^{+4.3}_{-4.3}$
2644	0.09	$1.48\cdot10^{-1}$	135	$^{+9.4}_{-7.9}$	$^{+4.1}_{-4.0}$	$^{+0.5}_{-0.5}$	$^{-1.3}_{+1.8}$	$^{-1.5}_{+1.4}$	$^{-0.3}_{+0.3}$	$^{+0.1}_{-0.1}$	$^{+2.4}_{-2.4}$	$^{+0.8}_{-0.8}$
	0.14	$7.74\cdot10^{-2}$	107	$^{+11}_{-8.8}$	$^{+3.9}_{-4.2}$	$^{+0.5}_{-0.6}$	$^{-2.1}_{+1.6}$	$^{-0.1}_{+0.1}$	$^{+0.1}_{-0.0}$	$^{+0.1}_{-0.1}$	$^{+2.4}_{-2.4}$	$^{+1.3}_{-1.3}$
	0.21	$4.65\cdot10^{-2}$	77	$^{+13}_{-10}$	$^{+4.7}_{-4.5}$	$^{+1.5}_{-0.6}$	$^{-2.0}_{+0.8}$	$^{-0.4}_{+1.9}$	$^{+0.2}_{-0.2}$	$^{+0.1}_{-0.1}$	$^{+2.4}_{-2.4}$	$^{+2.2}_{-2.2}$
	0.29	$2.58\cdot10^{-2}$	57	$^{+15}_{-12}$	$^{+4.8}_{-5.5}$	$^{+0.0}_{-1.8}$	$^{-1.6}_{+0.1}$	$^{-1.1}_{+0.7}$	$^{+1.2}_{-1.4}$	$^{+0.0}_{-0.0}$	$^{+2.4}_{-2.4}$	$^{+3.2}_{-3.2}$
	0.40	$1.11\cdot10^{-2}$	33	$^{+20}_{-15}$	$^{+6.4}_{-6.8}$	$^{+0.6}_{-0.5}$	$^{-0.0}_{+0.0}$	$^{-3.3}_{+2.4}$	$^{+1.2}_{-1.3}$	$^{+0.4}_{-0.4}$	$^{+2.4}_{-2.4}$	$^{+4.8}_{-4.8}$
3073	0.06	$1.24\cdot10^{-1}$	83	$^{+12}_{-9.8}$	$^{+3.9}_{-4.2}$	$^{+0.3}_{-0.6}$	$^{-2.4}_{+1.9}$	$^{+0.8}_{-0.0}$	$^{+0.4}_{-0.3}$	$^{+0.1}_{-0.1}$	$^{+2.4}_{-2.4}$	$^{+0.5}_{-0.5}$
	0.10	$8.34\cdot10^{-2}$	87	$^{+12}_{-9.6}$	$^{+4.1}_{-3.7}$	$^{+1.2}_{-0.8}$	$^{-0.9}_{+1.7}$	$^{-0.4}_{+0.8}$	$^{-0.4}_{+0.2}$	$^{+0.1}_{-0.1}$	$^{+2.4}_{-2.4}$	$^{+0.9}_{-0.9}$
	0.15	$5.79\cdot10^{-2}$	99	$^{+11}_{-9.0}$	$^{+3.9}_{-3.7}$	$^{+0.5}_{-0.3}$	$^{-0.7}_{+1.3}$	$^{-0.5}_{-0.4}$	$^{-0.2}_{+0.1}$	$^{+0.1}_{-0.1}$	$^{+2.4}_{-2.4}$	$^{+1.5}_{-1.5}$
	0.23	$2.52\cdot10^{-2}$	53	$^{+16}_{-12}$	$^{+4.4}_{-4.4}$	$^{+0.8}_{-0.2}$	$^{-0.6}_{+1.1}$	$^{-1.4}_{+0.9}$	$^{+0.6}_{-0.4}$	$^{+0.1}_{-0.1}$	$^{+2.4}_{-2.4}$	$^{+2.4}_{-2.4}$
	0.32	$1.79\cdot10^{-2}$	49	$^{+16}_{-12}$	$^{+5.8}_{-5.6}$	$^{+0.2}_{-0.9}$	$^{-2.2}_{+1.7}$	$^{-1.0}_{+2.6}$	$^{+0.7}_{-0.7}$	$^{+0.1}_{-0.1}$	$^{+2.4}_{-2.4}$	$^{+3.6}_{-3.6}$
	0.43	$5.58\cdot10^{-3}$	21	$^{+27}_{-17}$	$^{+7.1}_{-7.0}$	$^{+0.2}_{-0.6}$	$^{-1.0}_{+1.2}$	$^{-2.9}_{+2.9}$	$^{+1.2}_{-1.3}$	$^{+0.5}_{-0.5}$	$^{+2.4}_{-2.4}$	$^{+5.2}_{-5.2}$
3568	0.07	$6.73\cdot10^{-2}$	59	$^{+15}_{-12}$	$^{+4.0}_{-4.2}$	$^{+1.4}_{-0.9}$	$^{-2.2}_{+1.7}$	$^{+0.6}_{-0.7}$	$^{+0.3}_{-0.3}$	$^{+0.1}_{-0.1}$	$^{+2.4}_{-2.4}$	$^{+0.6}_{-0.6}$
	0.11	$4.68\cdot10^{-2}$	64	$^{+14}_{-11}$	$^{+3.8}_{-4.4}$	$^{+0.3}_{-1.2}$	$^{-2.3}_{+1.5}$	$^{-0.8}_{+0.6}$	$^{-0.1}_{+0.2}$	$^{+0.0}_{-0.0}$	$^{+2.4}_{-2.4}$	$^{+1.0}_{-1.0}$
	0.17	$3.15\cdot10^{-2}$	62	$^{+14}_{-11}$	$^{+4.0}_{-4.5}$	$^{+0.7}_{-0.2}$	$^{-2.4}_{+1.2}$	$^{+0.1}_{-0.7}$	$^{-0.2}_{+0.1}$	$^{+0.1}_{-0.1}$	$^{+2.4}_{-2.4}$	$^{+1.7}_{-1.7}$
	0.25	$2.06\cdot10^{-2}$	56	$^{+15}_{-12}$	$^{+4.8}_{-5.0}$	$^{+0.3}_{-0.6}$	$^{-1.6}_{+1.0}$	$^{-2.1}_{+1.9}$	$^{+0.5}_{-0.2}$	$^{+0.1}_{-0.1}$	$^{+2.4}_{-2.4}$	$^{+2.6}_{-2.6}$
	0.35	$8.84\cdot10^{-3}$	33	$^{+20}_{-15}$	$^{+5.8}_{-5.4}$	$^{+1.5}_{-0.4}$	$^{-0.7}_{-0.0}$	$^{-0.9}_{+1.9}$	$^{+0.6}_{-0.7}$	$^{+0.2}_{-0.2}$	$^{+2.4}_{-2.4}$	$^{+4.0}_{-4.0}$
	0.47	$4.14\cdot10^{-3}$	19	$^{+29}_{-18}$	$^{+8.0}_{-7.5}$	$^{+0.7}_{-0.4}$	$^{-0.5}_{+1.3}$	$^{-3.1}_{+3.6}$	$^{+1.8}_{-0.6}$	$^{+0.6}_{-0.6}$	$^{+2.4}_{-2.4}$	$^{+5.9}_{-5.9}$
4145	0.08	$5.56\cdot10^{-2}$	58	$^{+15}_{-11}$	$^{+5.4}_{-4.3}$	$^{+1.8}_{-1.0}$	$^{-2.3}_{+3.4}$	$^{+1.6}_{-0.6}$	$^{+0.5}_{-0.5}$	$^{+0.1}_{-0.1}$	$^{+2.4}_{-2.4}$	$^{+0.7}_{-0.7}$
	0.13	$3.04\cdot10^{-2}$	53	$^{+16}_{-12}$	$^{+4.5}_{-3.8}$	$^{+0.8}_{-0.4}$	$^{-1.2}_{+2.5}$	$^{-0.7}_{+0.4}$	$^{-0.3}_{+0.5}$	$^{+0.0}_{-0.0}$	$^{+2.4}_{-2.4}$	$^{+1.2}_{-1.2}$
	0.19	$1.74\cdot10^{-2}$	47	$^{+17}_{-12}$	$^{+4.0}_{-4.1}$	$^{+0.3}_{-0.6}$	$^{-1.3}_{+0.8}$	$^{-0.5}_{+1.0}$	$^{+0.1}_{+0.1}$	$^{+0.2}_{-0.2}$	$^{+2.4}_{-2.4}$	$^{+1.9}_{-1.9}$
	0.28	$1.05\cdot10^{-2}$	36	$^{+20}_{-14}$	$^{+6.1}_{-5.0}$	$^{+3.0}_{-0.7}$	$^{-1.3}_{+2.1}$	$^{-1.6}_{+1.9}$	$^{+0.1}_{-0.6}$	$^{+0.1}_{-0.1}$	$^{+2.4}_{-2.4}$	$^{+3.0}_{-3.0}$
	0.39	$5.24\cdot10^{-3}$	23	$^{+25}_{-17}$	$^{+6.0}_{-6.3}$	$^{+0.6}_{-1.3}$	$^{-1.3}_{+0.0}$	$^{-1.8}_{+1.7}$	$^{+0.8}_{-0.9}$	$^{+0.3}_{-0.3}$	$^{+2.4}_{-2.4}$	$^{+4.6}_{-4.6}$
	0.51	$1.21\cdot10^{-3}$	7	$^{+54}_{-25}$	$^{+8.6}_{-9.1}$	$^{+1.2}_{-0.9}$	$^{-2.4}_{+2.2}$	$^{-4.5}_{+3.2}$	$^{+1.4}_{-0.6}$	$^{+0.5}_{-0.5}$	$^{+2.4}_{-2.4}$	$^{+6.6}_{-6.6}$
4806	0.11	$2.12\cdot10^{-2}$	33	$^{+20}_{-15}$	$^{+3.7}_{-4.3}$	$^{+0.3}_{-2.0}$	$^{-1.6}_{+1.1}$	$^{+0.4}_{+0.7}$	$^{+0.1}_{-0.4}$	$^{+0.1}_{-0.1}$	$^{+2.4}_{-2.4}$	$^{+1.0}_{-1.0}$
	0.16	$2.12\cdot10^{-2}$	47	$^{+17}_{-12}$	$^{+4.1}_{-4.4}$	$^{+0.7}_{-2.2}$	$^{-1.1}_{+1.3}$	$^{-0.7}_{+1.2}$	$^{-0.4}_{+0.6}$	$^{+0.1}_{-0.1}$	$^{+2.4}_{-2.4}$	$^{+1.6}_{-1.6}$
	0.23	$8.94\cdot10^{-3}$	30	$^{+22}_{-15}$	$^{+4.4}_{-4.4}$	$^{+0.2}_{-0.2}$	$^{-1.5}_{+1.6}$	$^{-1.0}_{-0.2}$	$^{+0.3}_{+0.1}$	$^{+0.1}_{-0.1}$	$^{+2.4}_{-2.4}$	$^{+2.4}_{-2.4}$
	0.33	$5.20\cdot10^{-3}$	23	$^{+25}_{-17}$	$^{+5.8}_{-5.5}$	$^{+1.3}_{-0.3}$	$^{+0.8}_{+1.2}$	$^{-2.2}_{+2.3}$	$^{+0.1}_{-0.6}$	$^{+0.1}_{-0.1}$	$^{+2.4}_{-2.4}$	$^{+3.7}_{-3.7}$
	0.44	$1.88\cdot10^{-3}$	10	$^{+43}_{-23}$	$^{+7.0}_{-7.6}$	$^{+0.5}_{-1.3}$	$^{-1.2}_{+0.8}$	$^{-3.6}_{+2.8}$	$^{+0.6}_{-1.3}$	$^{+0.4}_{-0.4}$	$^{+2.4}_{-2.4}$	$^{+5.4}_{-5.4}$
	0.56	$6.34\cdot10^{-4}$	4	$^{+78}_{-29}$	$^{+10}_{-8.8}$	$^{+2.0}_{-1.0}$	$^{+1.1}_{+1.9}$	$^{-3.2}_{+5.0}$	$^{+0.2}_{+2.3}$	$^{+0.4}_{-0.4}$	$^{+2.4}_{-2.4}$	$^{+7.5}_{-7.5}$
5561	0.12	$1.44\cdot10^{-2}$	30	$^{+22}_{-15}$	$^{+4.0}_{-4.5}$	$^{+0.5}_{-2.4}$	$^{-1.3}_{+1.9}$	$^{-0.8}_{-0.4}$	$^{+0.3}_{+0.0}$	$^{+0.0}_{-0.0}$	$^{+2.4}_{-2.4}$	$^{+1.1}_{-1.1}$
	0.18	$8.24\cdot10^{-3}$	24	$^{+25}_{-16}$	$^{+5.1}_{-4.3}$	$^{+0.7}_{-0.5}$	$^{-1.8}_{+2.8}$	$^{-0.6}_{+1.6}$	$^{-0.7}_{+0.6}$	$^{+0.2}_{-0.2}$	$^{+2.4}_{-2.4}$	$^{+1.8}_{-1.8}$
	0.26	$5.46\cdot10^{-3}$	25	$^{+24}_{-16}$	$^{+5.3}_{-5.1}$	$^{+0.7}_{-0.6}$	$^{-2.3}_{+2.8}$	$^{-1.3}_{+1.1}$	$^{+0.3}_{-0.1}$	$^{+0.1}_{-0.1}$	$^{+2.4}_{-2.4}$	$^{+2.8}_{-2.8}$
	0.37	$2.41\cdot10^{-3}$	13	$^{+36}_{-21}$	$^{+5.7}_{-5.8}$	$^{+0.3}_{-0.4}$	$^{-0.5}_{+0.2}$	$^{-2.1}_{+1.6}$	$^{+0.1}_{-0.4}$	$^{+0.2}_{-0.2}$	$^{+2.4}_{-2.4}$	$^{+4.3}_{-4.3}$
	0.49	$7.28\cdot10^{-4}$	5	$^{+67}_{-28}$	$^{+9.0}_{-8.2}$	$^{+1.0}_{-0.5}$	$^{-1.9}_{+3.6}$	$^{-3.7}_{+3.9}$	$^{+1.2}_{+0.2}$	$^{+0.5}_{-0.5}$	$^{+2.4}_{-2.4}$	$^{+6.2}_{-6.2}$
	0.61	$< 1.52\cdot10^{-4}$	0									

Table 5. Continued

Q^2 (GeV^2)	x	$\mathrm{d}^2\sigma/\mathrm{d}x\mathrm{d}Q^2$ (pb/GeV^2)	N	δ_s (%)	δ_t (%)	δ_u (%)	δ_1 (%)	δ_2 (%)	δ_3 (%)	δ_4 (%)	δ_5 (%)	δ_6 (%)
6966	0.14	$6.39\cdot10^{-3}$	39	+19 −14	+4.9 −4.4	+2.1 −1.1	−2.4 +2.6	+0.3 −0.2	+0.2 −0.1	+0.0 −0.0	+2.4 −2.4	+1.3 −1.3
	0.21	$6.94\cdot10^{-3}$	53	+16 −12	+4.5 −4.4	+0.7 −0.3	−1.6 +1.7	−1.1 +1.3	−0.5 +0.5	+0.2 −0.2	+2.4 −2.4	+2.2 −2.2
	0.30	$1.94\cdot10^{-3}$	24	+25 −16	+5.1 −5.2	+0.5 −0.1	−1.1 +1.2	−1.9 +1.5	−0.1 +0.0	+0.1 −0.1	+2.4 −2.4	+3.3 −3.3
	0.41	$1.10\cdot10^{-3}$	16	+32 −19	+6.5 −6.4	+0.5 −0.3	−1.0 +1.4	−2.2 +2.3	+0.4 −0.4	+0.2 −0.2	+2.4 −2.4	+4.9 −4.9
	0.53	$3.39\cdot10^{-4}$	6	+60 −26	+9.2 −8.8	+0.7 −0.7	−1.1 +1.0	−4.1 +4.9	+0.8 −0.2	+0.5 −0.5	+2.4 −2.4	+6.9 −6.9
	0.69	$2.77\cdot10^{-5}$	1	+220 −30	+14 −13	+1.0 −0.9	−0.9 +0.8	−6.4 +8.6	−2.7 +3.1	+0.7 −0.7	+2.4 −2.4	+10 −10
9059	0.13	$3.71\cdot10^{-3}$	11	+40 −22	+7.7 −8.9	+0.3 −5.5	−3.5 +4.1	+5.4 −4.8	+0.5 −0.9	+0.5 −0.5	+2.4 −2.4	+1.2 −1.2
	0.19	$3.48\cdot10^{-3}$	28	+23 −16	+5.3 −5.1	+1.8 −0.6	−3.2 +3.2	−0.4 +0.4	+0.1 +0.3	+0.2 −0.2	+2.4 −2.4	+1.9 −1.9
	0.27	$1.73\cdot10^{-3}$	22	+26 −17	+4.9 −5.3	+0.7 −0.3	−2.8 +1.8	−0.7 +1.0	−0.4 +0.1	+0.2 −0.2	+2.4 −2.4	+2.9 −2.9
	0.38	$8.34\cdot10^{-4}$	16	+32 −19	+6.6 −6.5	+0.5 −0.3	−1.3 +1.2	−3.2 +3.3	+0.1 +0.2	+0.2 −0.2	+2.4 −2.4	+4.5 −4.5
	0.51	$1.47\cdot10^{-4}$	3	+96 −30	+8.6 −8.1	+0.7 −0.1	−0.9 +1.7	−3.2 +4.0	+0.5 −0.7	+0.4 −0.4	+2.4 −2.4	+6.6 −6.6
	0.64	$8.16\cdot10^{-5}$	2	+130 −32	+11 −11	+1.2 −0.5	−1.8 +2.2	−5.8 +5.1	−0.4 +0.1	+0.0 −0.0	+2.4 −2.4	+9.0 −9.0
	0.78	$< 2.25\cdot10^{-5}$	0									
	0.93	$< 4.38\cdot10^{-6}$	0									
15072	0.61	$3.58\cdot10^{-5}$	4	+78 −29	+10 −11	+2.3 −0.9	−2.0 +1.5	−6.7 +4.5	−0.1 +0.3	+0.3 −0.3	+2.4 −2.4	+8.4 −8.4
	0.75	$4.98\cdot10^{-6}$	1	+220 −30	+28 −13	+2.7 −0.7	−1.0 +2.0	−5.7 +25	−0.4 +0.2	+1.2 −1.2	+2.4 −2.4	+11 −11
	0.91	$< 7.42\cdot10^{-7}$	0									

Table 6. The integral cross section table for 99–00 e^+p NC scattering. The first two columns of the table contain the Q^2 and x_{edge} values for the bin, the third contains the measured cross section $\int_{x_{\mathrm{edge}}}^{1}\mathrm{d}^2\sigma/\mathrm{d}x\mathrm{d}Q^2$ corrected to the electroweak Born level or the upper limit in case of zero observed events, the fourth contains the number of events reconstructed in the bin, N, the fifth contains the statistical uncertainty, δ_s, and the sixth contains the total systematic uncertainty, δ_t. The right part of the table lists the total uncorrelated systematic uncertainty, δ_u, followed by the bin-to-bin correlated systematic uncertainties δ_1–δ_6 defined in the text. The upper (lower) numbers refer to the variation of the cross section, whereas the signs of the numbers reflect the direction of change in the cross sections. Note that the normalization uncertainty, δ_7, is not listed

Q^2 (GeV^2)	x_{edge}	$\int_{x_{\mathrm{edge}}}^{1}\mathrm{d}^2\sigma/\mathrm{d}x\mathrm{d}Q^2$ (pb/GeV^2)	N	δ_s (%)	δ_t (%)	δ_u (%)	δ_1 (%)	δ_2 (%)	δ_3 (%)	δ_4 (%)	δ_5 (%)	δ_6 (%)
648	0.22	$1.33\cdot10^{-1}$	106	+11 −8.8	+10 −5.9	+2.4 −2.3	+9.0 −2.4	+0.2 +0.0	−0.6 +1.4	+0.1 −0.1	+1.6 −1.6	+3.9 −3.9
761	0.24	$6.73\cdot10^{-2}$	212	+7.3 −6.4	+5.7 −6.7	+2.0 −3.0	+1.7 −3.2	+0.1 +0.0	−0.1 +0.4	+0.0 −0.0	+1.6 −1.6	+4.2 −4.2
891	0.26	$4.41\cdot10^{-2}$	288	+6.2 −5.5	+5.6 −5.6	+1.0 −1.0	−1.4 +1.6	+0.0 +0.0	−0.9 +0.3	+0.1 −0.1	+1.6 −1.6	+4.5 −4.5
1045	0.29	$2.50\cdot10^{-2}$	224	+7.1 −6.3	+6.2 −5.8	+1.2 −0.7	−1.6 +2.7	+0.1 +0.0	−0.4 +0.3	+0.1 −0.1	+1.6 −1.6	+4.7 −4.7
1224	0.31	$1.48\cdot10^{-2}$	157	+8.6 −7.3	+6.2 −6.5	+1.7 −1.0	−3.0 +1.5	+0.1 +0.0	−0.5 +1.1	+0.1 −0.1	+1.6 −1.6	+5.0 −5.0
1431	0.34	$9.52\cdot10^{-3}$	120	+10 −8.3	+6.7 −6.5	+0.3 −0.4	−2.3 +2.7	+0.0 −0.0	−0.8 +0.9	+0.1 −0.1	+1.6 −1.6	+5.4 −5.4
1672	0.36	$3.90\cdot10^{-3}$	59	+15 −12	+7.4 −7.3	+0.2 −0.7	−3.4 +3.3	+0.0 +0.0	−0.7 +1.4	+0.2 −0.2	+1.6 −1.6	+5.8 −5.8
1951	0.39	$2.64\cdot10^{-3}$	46	+17 −13	+7.9 −7.8	+0.9 −1.0	−3.5 +3.8	+0.0 +0.0	−1.0 +1.2	+0.2 −0.2	+1.6 −1.6	+6.2 −6.2
2273	0.43	$1.52\cdot10^{-3}$	29	+22 −15	+8.3 −8.0	+0.6 −0.7	−3.0 +3.7	+0.0 +0.0	−1.2 +1.0	+0.1 −0.1	+1.6 −1.6	+6.8 −6.8
2644	0.46	$9.16\cdot10^{-4}$	22	+26 −17	+8.3 −8.7	+1.4 −1.4	−3.6 +2.4	+0.0 +0.0	−0.9 +1.5	+0.2 −0.2	+1.6 −1.6	+7.2 −7.2
3073	0.50	$4.79\cdot10^{-4}$	13	+36 −21	+10 −10	+0.7 −0.3	−6.6 +5.8	+0.0 +0.0	−0.6 +0.9	+0.1 −0.1	+1.6 −1.6	+7.8 −7.8
3568	0.54	$2.27\cdot10^{-4}$	7	+54 −25	+9.7 −11	+1.1 −2.0	−5.8 +3.6	+0.0 +0.0	−2.0 +1.1	+0.1 −0.1	+1.6 −1.6	+8.5 −8.5
4145	0.58	$7.57\cdot10^{-5}$	3	+96 −30	+11 −11	+1.3 −2.2	−4.8 +5.4	+0.0 +0.0	−2.4 +2.3	+0.0 −0.0	+1.6 −1.6	+9.1 −9.1
4806	0.63	$7.05\cdot10^{-5}$	3	+96 −30	+13 −13	+5.4 −2.1	−7.1 +6.5	+0.0 +0.0	−3.6 +1.6	+0.2 −0.2	+1.6 −1.6	+10 −10
5561	0.68	$6.09\cdot10^{-5}$	3	+96 −30	+13 −13	+1.2 −3.4	−4.4 +5.3	+0.0 −0.1	−1.6 +3.5	+0.3 −0.3	+1.6 −1.6	+11 −11
6966	0.79	$< 4.07\cdot10^{-6}$	0									

6.2 Systematic uncertainties

Systematic uncertainties associated with the MC simulations were estimated by re-calculating the cross section after modifying the simulation to account for known uncertainties. Cut values were varied where this method was not applicable.

6.2.1 Uncorrelated systematic uncertainties

The following systematic uncertainties are either small or exhibit no bin-to-bin correlations:

- electron energy resolution in the MC simulation. The effect on the cross sections was evaluated by changing the resolution by ±1% in the MC. This resulted in ±1% effects over almost the full kinematic range. The effect increased to ±2% for the double-differential cross section in several low Q^2 bins and for several integrated cross section bins;
- electron angle. Uncertainties in the electron scattering-angle determination are known to be at most 1 mrad [11]. The resulting systematic effects on the cross-section measurement were at most 2%;
- electron-isolation requirement. Variation of the electron-isolation energy by ±2 GeV caused negligible effects in the measured cross section in the low-Q^2 region and 2.5% in the high-Q^2 region;
- FCAL alignment. The FCAL jet position was varied by ±0.5 cm in both X and Y directions. The resulting changes in the cross sections were negligible;
- reconstructed-vertex uncertainty. The cut on the reconstructed Z vertex was changed by ±2 cm; The uncertainties in the cross sections associated with this variation were negligible over the full kinematic range;
- background uncertainty. The estimated background from all sources was less than 1% and gave negligible uncertainty.

6.2.2 Correlated systematic uncertainties

The significant correlated systematic uncertainties are listed below and labeled for further reference. They were determined to result from the following sources:

- $\{\delta_1\}$ electron-energy scale. The systematic uncertainty resulting from uncertainty in the electron energy scale was checked by changing the energy scale by ±1%. This resulted in typically 2% systematic variations in the cross sections;
- $\{\delta_2\}$ jet-energy scale. The uncertainty in the cross sections arising from the measurement of the jet energy was checked by changing the energy scale by ±1%. The effect in the highest-x bins was negligible over the full Q^2 region. The uncertainty in the double-differential cross-section bins was 0%–7% for $0.1 < x < 0.7$;
- $\{\delta_3\}$ FCAL first inner ring (FIR) EMC energy scale. The effect of the FIR EMC energy scale uncertainty on the cross section was checked by changing the energy scale by ±5%, which gave 0%–3.5% uncertainty as x increased from 0.1 to 0.9;
- $\{\delta_4\}$ different PDFs. The uncertainty in the extracted cross section resulting from uncertainties in the shape of the PDFs at high x was checked by comparing the cross sections calculated from different sets: CTEQ4D, CTEQ6D, MRST99, ZEUS-S and ZEUS-JETS. The effect was less than 1% at low x and increased to 5% at high x;
- $\{\delta_5\}$ simulation of the hadronic final state and jet-selection procedure. The invariant k_T jet algorithm was replaced with a cone algorithm [26] with cone radius 0.7, and cross sections were re-evaluated. The uncertainty was found to be ±1.6% in the highest x bins and ±2.5% in the lower x bins. In addition, the analysis was redone under the following conditions: including multi-jet events for the events with $x < x_{\text{edge}}$; varying the jet E_T and θ_{jet} cuts for the jet selection; and varying the y_{JB} cut. These checks produced small differences consistent with expected statistical variations and were not included in the systematic uncertainty;
- $\{\delta_6\}$ higher order radiative corrections and a possible dependence on x. The uncertainty was estimated by evaluating the difference between assuming a constant for the leading order radiative correction as a function of x to assuming a second order polynomial. The difference observed at the leading order was used as the uncertainty coming from unknown higher order effects, and range from about 0.5% at the smallest x values to about 12% at the highest x values;
- $\{\delta_7\}$ uncertainties on the luminosity. The uncertainties for the 96–97 e^+p sample, 98–99 e^-p sample and 99–00 e^+p sample are 1.6%, 1.8% and 2.25%, respectively.

The systematic uncertainties were assumed fully correlated for the three data sets presented in this paper.

6.3 Results

The measured Born level cross sections for 96–97 e^+p, 98–99 e^-p and 99–00 e^+p and their systematic uncertainties are shown in Tables 1–6. The statistical uncertainties on the cross sections correspond to the central 68% probability interval evaluated using a Bayesian approach with flat prior and a Poisson likelihood. For bins with zero measured events, a 68% probability limit, calculated including the uncorrelated systematic uncertainty, is given. The cross sections are shown in Figs. 9–11 and compared to SM expectations using the CTEQ6M PDFs [3]. The double differential cross sections are represented by solid points, and generally agree well with the expectations. The cross section in the highest-x bins is plotted as

$$\frac{1}{1-x_{\text{edge}}}\int_{x_{\text{edge}}}^{1}\frac{\mathrm{d}^2\sigma_{\text{Born}}}{\mathrm{d}x\mathrm{d}Q^2}\mathrm{d}x\,.$$

In these bins, the expected cross section is drawn as a horizontal line, while the measured cross section is displayed as the open symbol at the center of the bin. The error bars represent the quadratic sum of the correlated systematic uncertainty and the combined statistical and uncorrelated systematic uncertainty determined from the Bayesian probability analysis.

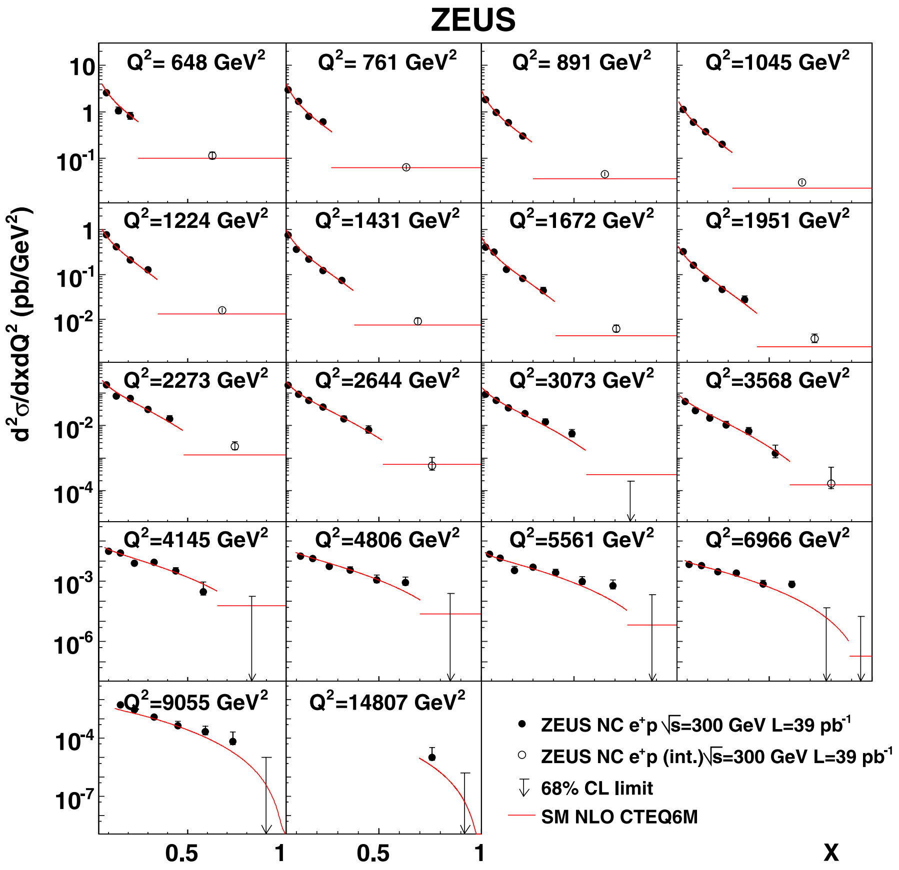

Fig. 9. The double-differential cross section for 96–97 e^+p NC scattering at $\sqrt{s} = 300$ GeV (*solid circles*) and the integral of the double differential cross section (*open circles*) compared to the standard model expectations evaluated using CTEQ6M PDFs (*lines*).The *error bars* show the statistical and systematic uncertainties added in quadrature. For bins with zero measured events, a 68% probability limit, calculated including the uncorrelated systematic uncertainty, is given

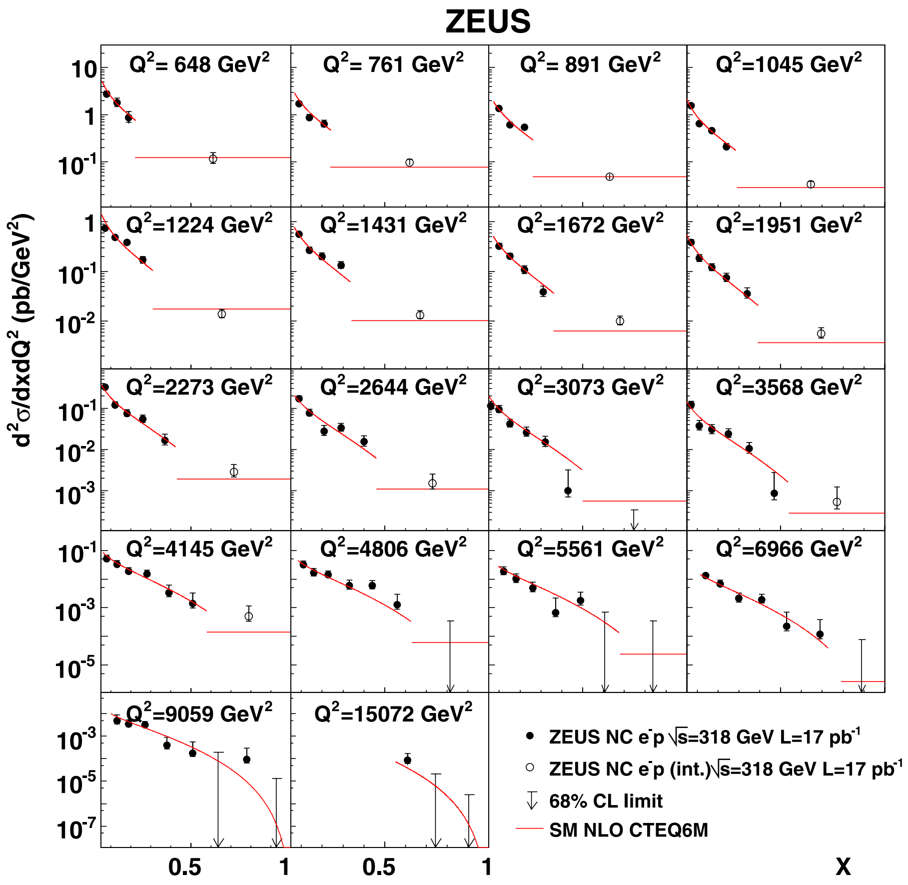

Fig. 10. The double-differential cross section for 98–99 e^-p NC scattering at $\sqrt{s} = 318$ GeV (*solid circles*) and the integral of the double differential cross section (*open circles*) compared to the standard model expectations evaluated using CTEQ6M PDFs (*lines*). The *error bars* show the statistical and systematic uncertainties added in quadrature. For bins with zero measured events, a 68% probability limit, calculated including the uncorrelated systematic uncertainty, is given

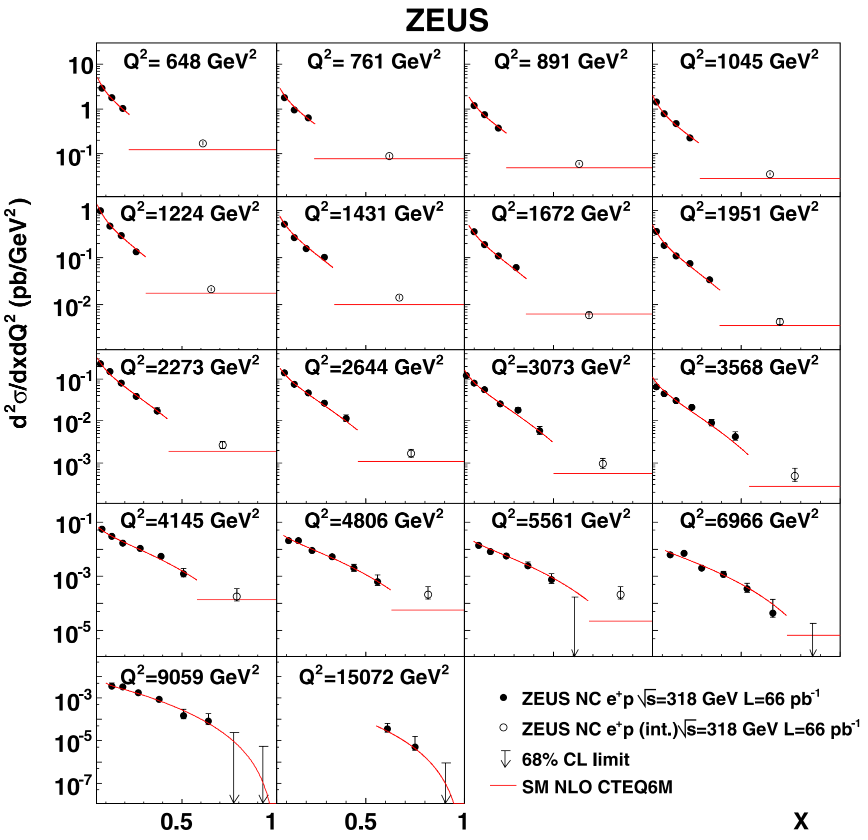

Fig. 11. The double-differential cross section for 99–00 e^+p NC scattering at $\sqrt{s} = 318$ GeV (*solid circles*) and the integral of the double differential cross section (*open circles*) compared to the standard model expectations evaluated using CTEQ6M PDFs (*lines*). The *error bars* show the statistical and systematic uncertainties added in quadrature. For bins with zero measured events, a 68% probability limit, calculated including the uncorrelated systematic uncertainty, is given

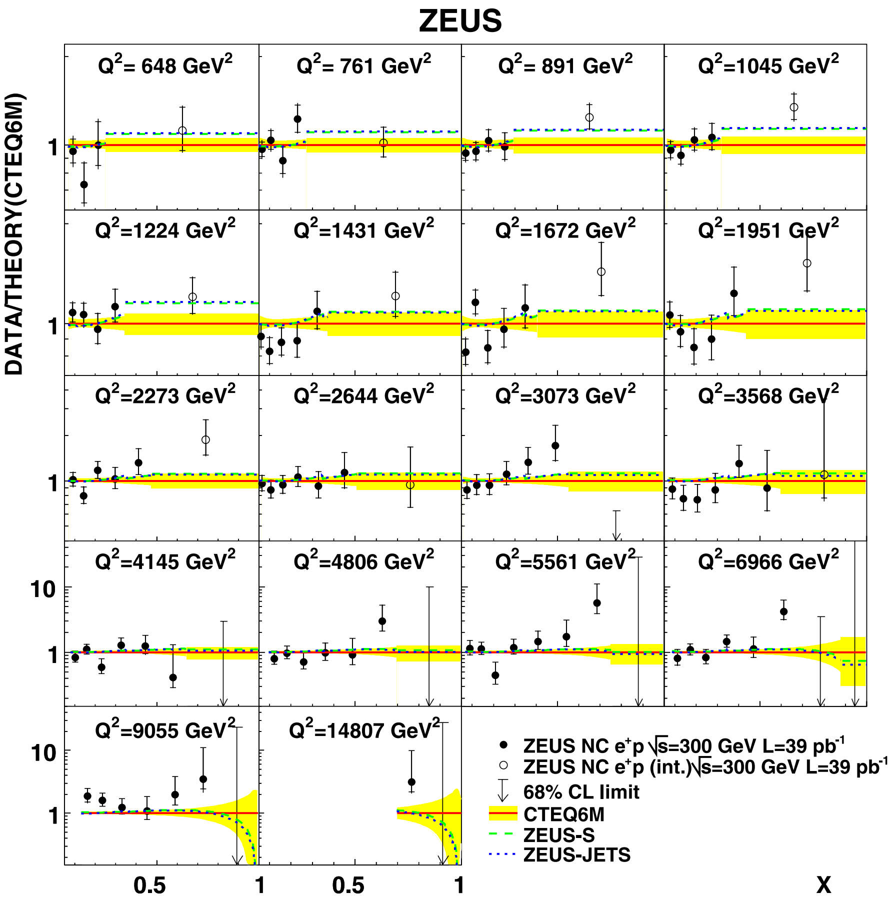

Fig. 12. Ratio of the double-differential cross section for 96–97 e^+p NC scattering (*solid circles*) and the integral of the double differential cross section (*open circles*) to the standard model expectation evaluated using the CTEQ6M PDFs. The *inner error bars* show the statistical uncertainty, while the outer ones show the statistical and systematic uncertainties added in quadrature. The ratio of the expectations using the ZEUS-S and ZEUS-JET PDFs to those using the CTEQ6M predictions are also shown. For bins with zero measured events, a 68% probability limit, calculated including the uncorrelated systematic uncertainty, is given

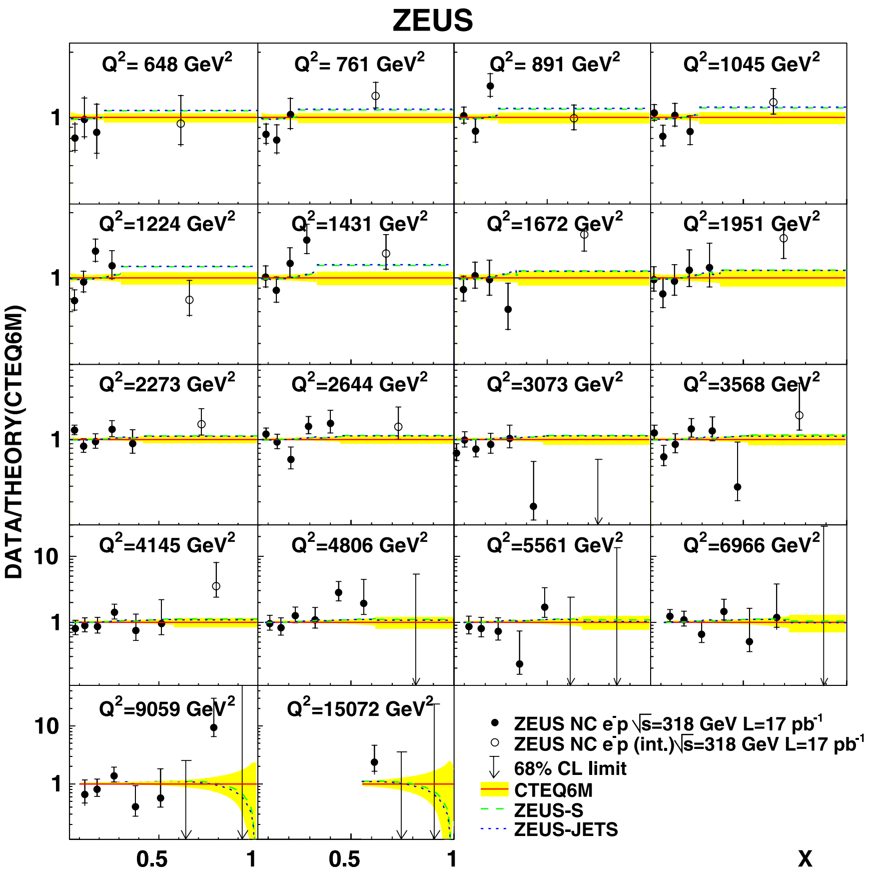

Fig. 13. Ratio of the double-differential cross section for 98–99 e^-p NC scattering (*solid circles*) and the integral of the double differential cross section (*open circles*) to the standard model expectation evaluated using the CTEQ6M PDFs. The *inner error bars* show the statistical uncertainty, while the outer ones show the statistical and systematic uncertainties added in quadrature. The ratio of the expectations using the ZEUS-S and ZEUS-JET PDFs to those using the CTEQ6M predictions are also shown. For bins with zero measured events, a 68% probability limit, calculated including the uncorrelated systematic uncertainty, is given

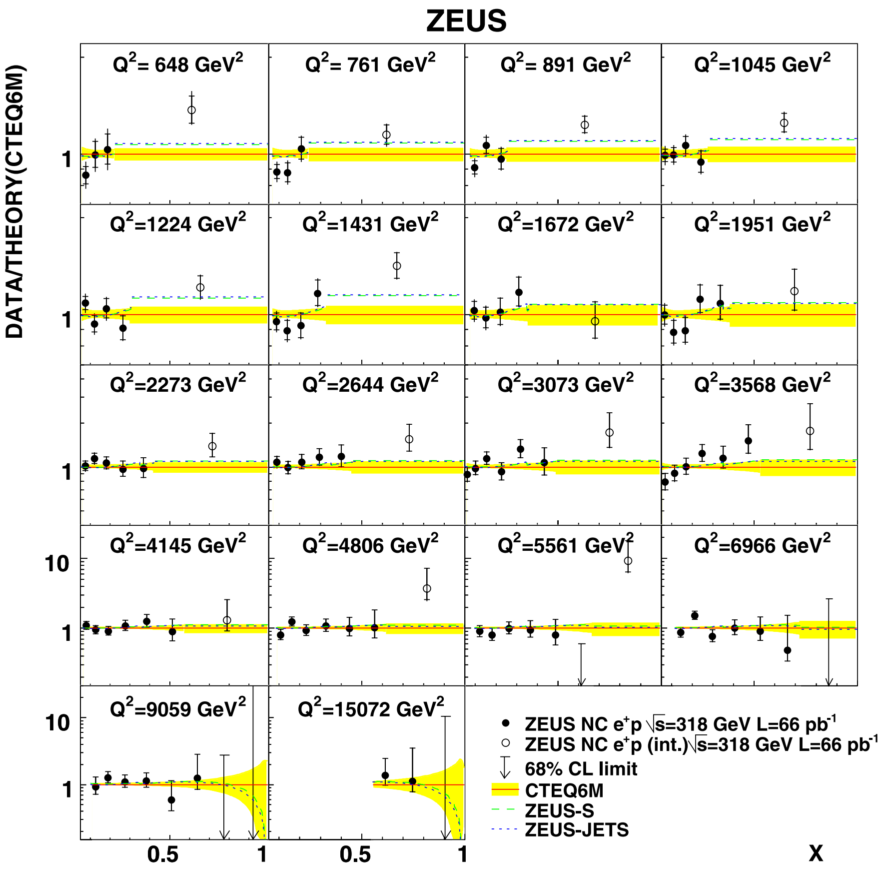

Fig. 14. Ratio of the double-differential cross section for 99–00 e^+p NC scattering (*solid circles*) and the integral of the double differential cross section (*open circles*) to the standard model expectation evaluated using the CTEQ6M PDFs. The *inner error bars* show the statistical uncertainty, while the outer ones show the statistical and systematic uncertainties added in quadrature. The ratio of the expectations using the ZEUS-S and ZEUS-JET PDFs to those using the CTEQ6M predictions are also shown. For bins with zero measured events, a 68% probability limit, calculated including the uncorrelated systematic uncertainty, is given

The ratios of the measured cross sections to the SM expectation using the CTEQ6M PDFs for 96–97 e^+p , 98–99 e^-p and 99–00 e^+p are shown in Figs. 12–14. The ratios of the expectations using the ZEUS-S PDF [39] to that using CTEQ6M and ZEUS-JETS PDF [40] to that using CTEQ6M are also shown. The uncertainty for the CTEQ6M fit is displayed in the figure as a shaded band. The measured double-differential cross sections generally agree well with all three sets of expectations. For the highest x bins, which extend to previously unmeasured kinematic ranges, the data have a tendency to lie above the expectations.

The data presented here, specifically the zero-jet data at high x, extend the kinematic coverage for DIS. These results are expected to have a significant impact on the valence-quark distributions at high x, where little data are available to date. It should however be noted that there is overlap with the data presented in previous ZEUS publications, and these new results should therefore not be used simultaneously with the previously published ZEUS data [4, 10, 11] in fits to extract model parameters. In the kinematic region of overlap of this technique with the previous ZEUS technique, the extracted cross sections are in excellent agreement.

7 Summary

This paper has presented a reanalysis of previously published ZEUS data with a new technique designed for the reconstruction of large x events, which allows for the extraction of the cross section up to $x = 1$. In the previously measured kinematic region, the data and simulation based on the CTEQ6M PDF are in good agreement. The Standard Model predictions tend to underestimate the data at the highest values of x.

Acknowledgements. We are grateful to the DESY directorate for their strong support and encouragement. We thank the HERA machine group whose outstanding efforts allowed the measurements presented here. We also wish to express our thanks for the support of the DESY computing and network services. The design, construction and installation of the ZEUS detector has been made possible by the efforts of many people not listed as authors.

References

1. J.D. Bjorken, E.A. Paschos, Phys. Rev. **185**, 1975 (1969)
2. A.D. Martin et al., Phys. Lett. B **531**, 216 (2002)
3. J. Pumplin et al., JHEP **0207**, 012 (2002)
4. ZEUS Collaboration, S. Chekanov et al., Phys. Rev. D **70**, 052 001 (2003)
5. H1 Collaboration, C. Adloff et al., Eur. Phys. J. C **30**, 1 (2003)
6. S. Alekhin, Phys. Rev. D **68**, 014 002 (2003)
7. BCDMS Collaboration, A.C. Benvenuti et al., Phys. Lett. B **223**, 485 (1989)
8. L.W. Whitlow et al., Phys. Lett. B **282**, 475 (1992)
9. M. Osipenko et al., Phys. Rev. D **67**, 092 001 (2003)
10. ZEUS Collaboration, S. Chekanov et al., Eur. Phys. J. C **21**, 443 (2001)
11. ZEUS Collaboration, S. Chekanov et al., Eur. Phys. J. C **28**, 175 (2003)
12. ZEUS Collaboration, U. Holm (ed.), The ZEUS Detector. Status Report (unpublished), DESY (1993), available on http://www-zeus.desy.de/bluebook/bluebook.html
13. M. Derrick et al., Nucl. Instrum. Methods A **309**, 77 (1991)
14. A. Andresen et al., Nucl. Instrum. Methods A **309**, 101 (1991)
15. A. Caldwell et al., Nucl. Instrum. Methods A **321**, 356 (1992)
16. A. Bernstein et al., Nucl. Instrum. Methods A **336**, 23 (1993)
17. N. Harnew et al., Nucl. Instrum. Methods A **279**, 290 (1989)
18. B. Foster et al., Nucl. Phys. B Proc. Suppl. **32**, 181 (1993)
19. B. Foster et al., Nucl. Instrum. Methods A **338**, 254 (1994)
20. J. Andruszków et al., Preprint DESY-92-066, DESY, 1992
21. ZEUS Collaboration, M. Derrick et al., Z. Phys. C **63**, 391 (1994)
22. J. Andruszków et al., Acta Phys. Pol. B **32**, 2025 (2001)
23. ZEUS Collaboration, J. Breitweg et al., Eur. Phys. J. C **11**, 427 (1999)
24. S. Catani et al., Nucl. Phys. B **406**, 187 (1993)
25. S.D. Ellis, D.E. Soper, Phys. Rev. D **48**, 3160 (1993)
26. J.E. Huth et al., Research Directions for the Decade. Proceedings of Summer Study on High Energy Physics, 1990, E.L. Berger (ed.), (World Scientific, 1992), p. 134, Also in preprint FERMILAB-CONF-90-249-E
27. ZEUS Collaboration, J. Breitweg et al., Eur. Phys. J. C **16**, 253 (2000)
28. Y. Ning, Ph.D. Thesis, Columbia University, (2006), (unpublished)
29. G.A. Schuler, H. Spiesberger, Proc. Workshop on Physics at HERA, W. Buchmüller, G. Ingelman (eds.), Vol. 3, p. 1419. Hamburg, Germany, DESY (1991)
30. H. Spiesberger, HERACLES, DJANGOH: Event Generation for *ep* Interactions at HERA Including Radiative Processes, 1998, available on http://www.desy.de/~hspiesb/djangoh.html
31. A. Kwiatkowski, H. Spiesberger, H.-J. Möhring, Comput. Phys. Commun. **69**, 155 (1992)
32. G. Ingelman, A. Edin, J. Rathsman, Comput. Phys. Commun. **101**, 108 (1997)
33. T. Sjöstrand, Comput. Phys. Commun. **82**, 74 (1994)
34. R. Brun et al., GEANT3, Technical Report CERN-DD/EE/84-1, CERN, 1987
35. ZEUS Collaboration, S. Chekanov et al., Eur. Phys. J. C **32**, 1 (2003)
36. X. Liu, Ph.D. Thesis, Columbia University, (2003), (unpublished)
37. F. Jacquet, A. Blondel, Proceedings of the Study for an *ep* Facility for Europe, U. Amaldi (ed.), (Hamburg, Germany 1979), p. 391, Also in preprint DESY 79/48
38. A. Arbuzov et al., Comput. Phys. Commun. **94**, 128 (1996)
39. ZEUS Collaboration, S. Chekanov et al., Phys. Rev. D **67**, 12 007 (2003)
40. ZEUS Collaboration, S. Chekanov et al., Eur. Phys. J. C **42**, 1 (2005)